Atmos. Chem. Phys., 24, 1801–1824, 2024
https://doi.org/10.5194/acp-24-1801-2024

Atmospheric Chemistry and Physics
Open Access
EGU

Higher absorption enhancement of black carbon in summer shown by 2-year measurements at the high-altitude mountain site of Pic du Midi Observatory in the French Pyrenees

Sarah Tinorua[1], Cyrielle Denjean[1], Pierre Nabat[1], Thierry Bourrianne[1], Véronique Pont[2], François Gheusi[2], and Emmanuel Leclerc[2]

[1]CNRM, Université de Toulouse, Météo-France, CNRS, Toulouse, France
[2]Laboratoire d'Aérologie, Université Toulouse III – Paul Sabatier (UPS), CNRS (UMR 5560), Toulouse, France
Correspondence: Sarah Tinorua (sarah.tinorua@umr-cnrm.fr) and Cyrielle Denjean (cyrielle.denjean@meteo.fr)

Received: 24 March 2023 – Discussion started: 11 April 2023
Revised: 8 December 2023 – Accepted: 10 December 2023 – Published: 8 February 2024

Abstract. Black-carbon-containing particles strongly absorb light, causing substantial radiative heating of the atmosphere. The climate-relevant properties of black carbon (BC) are poorly constrained in high-altitude mountain regions, where many complex interactions between BC, radiation, clouds and snow have important climate implications. This study presents 2-year measurements of BC microphysical and optical properties at the Pic du Midi (PDM) research station, a high-altitude observatory located at 2877 m above sea level in the French Pyrenees. Among the long-term monitoring sites in the world, PDM is subject to limited influence from the planetary boundary layer (PBL), making it a suitable site for characterizing the BC in the free troposphere (FT).

The classification of the dominant aerosol type using aerosol spectral optical properties indicates that BC is the predominant aerosol absorption component at PDM and controls the variation in single-scattering albedo (SSA) throughout the 2 years. Single-particle soot photometer (SP2) measurements of refractory BC (rBC) show a mean mass concentration (M_{rBC}) of 35 ng m^{-3} and a relatively constant rBC core mass-equivalent diameter of about 180 nm, which are typical values for remote mountain sites. Combining the M_{rBC} with in situ absorption measurements, a rBC mass absorption cross-section (MAC_{rBC}) of 9.2 ± 3.7 m^2 g^{-1} at $\lambda = 880$ nm has been obtained, which corresponds to an absorption enhancement (E_{abs}) of ~ 2.2 compared to that of bare rBC particles with equal rBC core size distribution. A significant reduction in the $\Delta M_{rBC}/\Delta CO$ ratio when precipitation occurred along the air mass transport suggests wet removal of rBC. However we found that the wet removal process did not affect the rBC size, resulting in unchanged E_{abs}. We observed a large seasonal contrast in rBC properties with higher M_{rBC} and E_{abs} in summer than in winter. In winter a high diurnal variability in M_{rBC} (E_{abs}) with higher (lower) values in the middle of the day was linked to the injection of rBC originating from the PBL. On the contrary, in summer, M_{rBC} showed no diurnal variation despite more frequent PBL conditions, implying that M_{rBC} fluctuations are rather dominated by regional and long-range transport in the FT. Combining the $\Delta M_{rBC}/\Delta CO$ ratio with air mass transport analysis, we observed additional sources from biomass burning in summer leading to an increase in M_{rBC} and E_{abs}. The diurnal pattern of E_{abs} in summer was opposite to that observed in winter with maximum values of ~ 2.9 observed at midday. We suggest that this daily variation may result from a photochemical process driving the rBC mixing state rather than a change in BC emission sources.

Such direct 2-year observations of BC properties provide quantitative constraints for both regional and global climate models and have the potential to close the gap between model-predicted and observed effects of BC on the regional radiation budget and climate. The results demonstrate the complex influence of BC emission sources, transport pathways, atmospheric dynamics and chemical reactivity in driving the light absorption of BC.

Published by Copernicus Publications on behalf of the European Geosciences Union.

1 Introduction

Black carbon (BC) is a light-absorbing carbonaceous aerosol produced by incomplete combustion of fossil fuels, including not only anthropogenic emissions from traffic, residential heating and cooking, power plants, and industries but also natural emissions such as biomass burning (Bond et al., 2013; Bond and Bergstrom, 2006). Recent scientific assessments of the sixth IPCC (Intergovernmental Panel on Climate Change) report (Szopa et al., 2021) estimate that BC is the most absorbing atmospheric aerosol with a best estimate of effective radiative forcing around $+0.107\,\mathrm{W\,m^{-2}}$, thereby increasing the global mean surface air temperature by 0.063 °C for the period 1750–2019 (Szopa et al., 2021). The contribution of BC to climate change is estimated to be among the highest uncertainties ($\sim 90\,\%$) in climate models, limiting their accuracy (Bellouin et al., 2020). The large uncertainty in BC direct radiative forcing due to BC–radiation interactions can be attributed, in addition to uncertainties in BC emissions and lifetime, to variations in BC optical properties that are neglected by climate models (Matsui et al., 2018).

A crucial factor in estimating the BC radiative effect is the mass absorption cross-section ($\mathrm{MAC_{BC}}$), which is defined as the light-absorption-equivalent cross-section of BC per unit of mass concentration (M_{BC}). The $\mathrm{MAC_{BC}}$ can be calculated either by dividing the measured absorption coefficient of BC by its mass concentration or by using Mie's theory and the BC size distribution and coating thickness as input variables. Observations show that the BC radiative forcing is likely underestimated by around 10 % to 40 % in current climate models due to too low a simulated $\mathrm{MAC_{BC}}$ (Bond et al., 2013; Boucher et al., 2016; Matsui et al., 2018; Myhre and Samset, 2015). In situ measurements of $\mathrm{MAC_{BC}}$ have reported a wide range of values, from 3.8 to $58\,\mathrm{m^2\,g^{-1}}$ (Wei et al., 2020). Although such high variability can be attributed, in part, to the determination method of the $\mathrm{MAC_{BC}}$ based on M_{BC} and absorption measurement techniques, differences in $\mathrm{MAC_{BC}}$ values were found even for the same measurement technique.

Values of $\mathrm{MAC_{BC}}$ depend on BC microphysical and chemical properties, which are related to their emission sources (Schwarz et al., 2008) and the effects of aging processes during transport in the atmosphere (Ko et al., 2020; Laborde et al., 2013; Sedlacek et al., 2022). Freshly emitted BC is made of porous, fractal-like aggregates of nanoparticles (Beeler and Chakrabarty, 2022; China et al., 2013) that can become coated by condensation and/or coagulation with non-BC components (such as sulfate, nitrate and organic components) during atmospheric aging (Fierce et al., 2020). Conversely this coating can be removed through evaporation and/or chemical processing via the production of more volatile substances (Sedlacek et al., 2022). Numerous studies have demonstrated that coating of BC with non-absorbing materials is accompanied by an enhancement of light absorption (E_{abs}) through the so-called lensing effect (Cappa et al., 2012; Denjean et al., 2020; Yuan et al., 2021; Healy et al., 2015; Liu et al., 2015; McMeeking et al., 2014; Peng et al., 2016; Van de Hulst, 1957; Xie et al., 2019; Schwarz et al., 2006; Yus-Díez et al., 2022). However, most of these measurements were performed in the planetary boundary layer (PBL) and over short periods from a few hours to as long as a season.

Both observations and model simulations pointed out an amplification of the warming rate by greenhouse gases and absorbing aerosols at high mountain sites compared to PBL areas (Gao et al., 2018; Liu et al., 2009; Pepin et al., 2019; Rangwala, 2013). López-Moreno et al. (2014) have shown by running several regional climate models that the occurrence of winter warm events in the Spanish Pyrenees will gradually increase until 2080. This includes an increase in the number of warm days and nights and the number of snow/ice melting days at altitudes above 2000 m above sea level (m a.s.l.). This so-called elevation-dependent warming (EDW) has been reviewed by the Mountain Research Initiative EDW Working Group, 2015, who listed the possible mechanisms behind this phenomenon (Pepin et al., 2015). Among the reasons given, BC is a potential driver of EDW by both absorbing solar radiation in the troposphere and decreasing the surface albedo when deposited on the cryosphere, thereby accelerating snowmelt (Réveillet et al., 2022). In addition, BC has been found to have a higher radiative effect when it is located above clouds rather than near the surface (Samset and Myhre, 2015; Sanroma et al., 2010). All these findings highlight the importance of studying BC at high-altitude mountain sites, where its effects on climate could be even more significant.

This study presents 2-year continuous measurements of BC and aerosol properties conducted during the hygroscopic properties of black carbon (h-BC) campaign at the high-altitude long-term monitoring station Pic du Midi (PDM). Located at 2877 m a.s.l. in the French Pyrenees, PDM has been long identified as a clean remote station (Marenco et al., 1994).

This paper aims to provide a comprehensive picture of the seasonal and diurnal variability in refractory BC (rBC) properties at PDM and to explore the processes driving these properties. Specifically, the following questions are addressed:

1. What are the air mass transport pathways impacting PDM?
2. What is the seasonal variability in aerosol optical properties and dominant aerosol types? What is the specific contribution of rBC to aerosol absorption?
3. How do the microphysical and optical properties of rBC vary on a seasonal and daily basis?

4. What are the roles of wet deposition, the source and the transport pathway in driving rBC absorption?

2 Methods

2.1 Measurement site and observation period

Measurements were performed at the Pic du Midi (PDM; 42.9° N, 0.1° E; 2877 m a.s.l.) mountain research station in the French Pyrenees. This station is part of the Pyrenean Platform for Observation of the Atmosphere (P2OA).[1]

As shown in Fig. 1, the site is located 150 km east of the Atlantic coast. The high isolated summit lies around 20 km north of the main ridge of the Pyrenees (on the France–Spain border) and thus closely overlooks the French plain. Using a backward particle dispersion model, Henne et al. (2010) found the influence of local anthropogenic emissions to be very limited at PDM and classified the station in the "mostly remote" category. Collaud Coen et al. (2018) defined an "ABL-Topoindex" as a metric of the atmospheric boundary layer influence for a mountain site. PDM has been found to have a low ABL-Topoindex, similar to other Alpine high-altitude stations. PDM is thus a suitable site to study both the background lower free troposphere (FT) over long timescales and the injection of air masses from the PBL (Hulin et al., 2019; Tsamalis et al., 2014; Fu et al., 2016; Marusczak et al., 2017). Long-term monitoring of numerous meteorological, gas and aerosol parameters has been conducted for nearly 2 decades, notably through the Global Atmosphere Watch (GAW) program of the World Meteorological Organization (WMO), as well as the national research infrastructure ACTRIS-France. Results from the h-BC campaign performed from February 2019 to January 2021 at PDM (in addition to the routine measurements) are presented in this paper.

2.2 Instrumentation

2.2.1 Total inlet

All particle-measuring instruments sampled air taken in parallel from a whole air inlet, located 2 m above the building roof. This inlet is used for the long-term observations in mountainous sites and is designed to maintain an isokinetic and laminar flow. The main flow rate was fixed at about 460 L min^{-1}. The splitter was fixed at the end of the stainless tube. The hat of the whole air inlet and the stainless tube were both thermo-regulated in order to avoid frost and gradually regulate the temperature of the sampled air to the measurement room. The air was heated to around 20 °C in order to perform aerosol in situ measurements at a relative humidity lower than 30 %. The instrumental room temperature was regulated at around 20 °C. The annual cycle of the dew point temperature varied between about −10 and +5 °C.

[1] http://p2oa.aeris-data.fr (last access: 23 January 2024).

2.2.2 Black carbon measurements

BC can be measured by different methods which are based on different BC properties. Petzold et al. (2013) defined a specific nomenclature for BC according to the BC quantification method. Following the recommendation of the authors, BC quantified by laser-induced incandescence, filter-based absorption and thermal–optical analysis will be referred to as refractory black carbon (rBC), equivalent black carbon (eBC) and elemental carbon (EC), respectively. More general discussion on BC without focusing on its measurement technique will be referred to as BC. The mass concentration of rBC and rBC size distribution were measured by a single-particle soot photometer (SP2; Droplet Measurement Technologies, Longmont, CO, USA). Its operating principles have been described in previous articles (Gao et al., 2007; Moteki and Kondo, 2007; Schwarz et al., 2006). In short, this instrument uses a laser-induced incandescence technique which quantifies rBC mass in single particles. A continuous intracavity laser beam (Nd:YAG; $\lambda = 1064$ nm) is used to heat rBC-containing particles to their vaporization point. The measured incandescence signal of an individual rBC-containing particle can be converted to a rBC mass, using a calibration curve obtained by recording the incandescence signal peak height of mobility size-selected fullerene soot (Alfa Aesar, lot no. FS12S011) and assuming a BC mass density of 1.8 g cm^{-3} (Moteki and Kondo, 2010). This calibration was performed twice a year and did not change during the 2 years of the measurement campaign.

The SP2 data were processed using a Python code following the method used in the SP2 Toolkit from the Paul Scherrer Institute (Gysel et al., 2009). A comparison of M_{rBC} resulting from the SP2 Toolkit with our Python processing is presented in Text S1 in the Supplement. The SP2 used in this study measured rBC cores over a size range between 90 and 580 nm. However, the observed size distributions showed that an important fraction (around 12 %) of M_{rBC} at diameters below 90 nm is not measured by the SP2 (Fig. S2 in the Supplement). Because of these small-mode particles outside the SP2 detection range, the quantification of M_{rBC} could be underestimated. To compensate for the missing mass, the observed rBC size distributions have been fitted daily using the sum of three individual lognormal distributions to extrapolate rBC size distribution in the range of 1 to 1000 nm. The positions of the three modes were constrained in the following ranges: Mode 1, $50 < D_{\mathrm{g}} < 100$ nm and $1.2 < \sigma_{\mathrm{g}} < 3$; Mode 2, $150 < D_{\mathrm{g}} < 250$ nm and $1.3 < \sigma_{\mathrm{g}} < 2.9$; and Mode 3, $350 < D_{\mathrm{g}} < 500$ nm and $1 < \sigma_{\mathrm{g}} < 3$, with D_{g} and σ_{g} the geometric mean diameter and the geometric standard deviation, respectively. Using the fitting procedure, a time-dependent missing mass correction was applied to the observed M_{rBC} to calculate the overall M_{rBC}. The average missing mass correction factor over the campaign was 1.2 ± 1.1 (mean value ± SD). More details on the SP2 data procedure can be found in Text S2 in the Supplement. The

Figure 1. Geographical location of the Pic du Midi Observatory in the French Pyrenees (© IGN and © Google Earth).

extent to which the uncertainty in this fitting procedure contributes to the overall M_{rBC} was quantified by comparing the M_{rBC} calculated from the observed BC size distribution and the fit curve over the SP2 size range. An excellent match was obtained between the measured and fitted size distribution, resulting in differences of less than 0.2 %. The combined uncertainty in the M_{rBC} was estimated to be about 24.5 % by calculating the quadratic sum of the measurement uncertainties in sampling flow, anisokinetic sampling errors and the missing mass correction factor.

2.2.3 Aerosol properties

A scanning mobility particle sizer (SMPS), combining a differential mobility analyzer (DMA; model 3071, TSI Inc., Shoreview, MN, USA) and a condensation particle counter (CPC; model 3772, TSI Inc., Shoreview, MN, USA), allowed for the determination of aerosol size distribution between 12.6 and 532.6 nm.

Aerosol scattering coefficients (σ_{sca}) at three wavelengths (450, 525 and 635 nm) were measured with an integrating nephelometer (model Aurora 3000, Ecotech Pty Ltd, Knoxfield, Australia). A calibration with carbon dioxide and filtered air was performed every 3 months. The instrument measures σ_{sca} in the angular range 10–170°, and the correction of Müller et al. (2011) was used to account for the angular truncation errors.

Aerosol absorption coefficients (σ_{abs}) were measured by a seven-wavelength Aethalometer (model AE33, Magee Scientific Company, Berkeley, CA, USA; measuring wavelengths: 370, 470, 520, 590, 660, 880 and 950 nm). This instrument measures light attenuation through a filter on which aerosol sample is deposited. The Aethalometer filter loading effect was corrected online by the dual-spot manufacturer correction proposed by Drinovec et al. (2015). The multiple-scattering parameter used to correct the measured attenuation was set to 3.22, according to the value obtained at $\lambda = 880$ nm by Yus-Díez et al. (2021) at the mountainous site of Montsec d'Ares located less than 200 km from the PDM (see the Table S3 in the Supplement of Yus-Díez et al., 2021). Uncertainty in the corrected σ_{abs} was estimated to be 35 % (Zanatta et al., 2016). The detection limit of the Aethalometer is 0.039 Mm^{-1} (corresponding to an equivalent black carbon mass concentration of 0.005 $\mu g\,m^{-3}$).

2.2.4 Gas-phase measurements

Two different instruments have been deployed to measure carbon monoxide (CO) with a final time resolution of 1 h: an IR-absorption analyzer (model 48CTL, Thermo Environmental Instruments (TEI), New Delhi, India) placed close to the aerosol instrumentation in order to detect pollution plumes produced locally at PDM and a cavity ring-down spectrometer (CRDS; model G2401, Picarro, Santa Clara, CA, USA), located in an other building, used to measure the background carbon monoxide (CO) concentration (see Sect. 2.3).

A key issue in our study is the distinction between FT- and PBL-influenced air masses. Optical properties of BC depend on its aging and transport pathways in the atmosphere, so it is crucial to determine whether it has been transported over the PBL or in the FT. For this purpose, we routinely monitor the diurnal cycle of radon (^{222}Rn) volumetric activity at PDM with a 1500 L high-sensitivity radon monitor (model D1500, Australian Nuclear Science and Technology Organisation (ANSTO), Australia) (Whittlestone and Zahorowski, 1998). Radon is an inert radioactive gas emitted from ice-free soils with a half-life of 3.8 d, making it the most reliable tracer to discriminate between the FT- and PBL-influenced air masses (Chambers et al., 2013).

2.3 Determination of intensive aerosol and BC properties

The spectral dependence of σ_{abs} was characterized by the absorption Ångström exponent ($AAE_{aer,450–635}$) calculated between 450 and 635 nm as follows:

$$AAE_{aer,450–635} = \frac{-\log\left(\frac{\sigma_{abs,450}}{\sigma_{abs,635}}\right)}{\left(\log\left(\frac{450}{635}\right)\right)}. \quad (1)$$

For this calculation, $\sigma_{abs,470}$ and $\sigma_{abs,660}$ from the Aethalometer were adjusted at the wavelengths of 450 and 635 nm measured by the nephelometer using the AAE calculated from the Aethalometer between 370–470 nm and 590–660 nm. $AAE_{aer,450–635}$ provides information about the chemical composition of atmospheric aerosols. Pure BC absorbs radiation across the whole solar spectrum with the same efficiency; thus, it is characterized by an $AAE_{aer,450–635}$ of around 1 (Bond et al., 2013). Conversely light-absorbing organic particles known as brown carbon (BrC), as well as dust particles, generally have an $AAE_{aer,450–635}$ greater than 2 (Sun et al., 2007; Bergstrom et al., 2007; Schuster et al., 2016).

The wavelength dependence of σ_{sca} can be characterized by the scattering Ångström exponent ($SAE_{aer,450–635}$) calculated between 450 and 635 nm as

$$SAE_{aer,450–635} = \frac{-\log\left(\frac{\sigma_{sca,450}}{\sigma_{sca,635}}\right)}{\left(\log\left(\frac{450}{635}\right)\right)}. \quad (2)$$

$SAE_{aer,450–635}$ describes the relative contribution of fine- and coarse-mode particles (Clarke and Kapustin, 2010). Small values of $SAE_{aer,450–635}$ indicate a higher contribution of large aerosol particles (e.g., dust and sea salt), while large values of $SAE_{aer,450–635}$ indicate relatively small aerosol particles (Cappa et al., 2016).

The aerosol single-scattering albedo ($SSA_{aer,\lambda}$) was calculated at the wavelengths of $\lambda = 450$, 525 and 635 nm using the following equation:

$$SSA_{aer,\lambda} = \frac{\sigma_{sca,\lambda}}{\sigma_{sca,\lambda} + \sigma_{abs,\lambda}}. \quad (3)$$

$SSA_{aer,\lambda}$ describes the relative importance of scattering and absorption to the total light extinction. Thus, it indicates the potential of aerosols to cool or warm the atmosphere. To calculate $SSA_{aer,\lambda}$, σ_{abs} was first calculated at the proper wavelength λ using the AAE calculated at the closest wavelengths ($AAE_{aer,370–470}$ to retrieve $\sigma_{abs,450}$, $AAE_{aer,520–590}$ for the $\sigma_{abs,525}$ and $AAE_{aer,590–660}$ for the $\sigma_{abs,635}$).

The $\Delta M_{rBC}/\Delta CO$ emission ratio was calculated to provide information on the combustion sources, as well as on BC wet deposition (Baumgardner et al., 2002). First, the background CO concentrations were estimated by taking the rolling 5th percentile of the values in a 14 d time window and then calculating a monthly mean (see Fig. S3 in the Supplement) based on the method of Kanaya et al. (2016). ΔCO was then calculated by subtracting the monthly background CO concentration for any measured hourly CO value. ΔM_{rBC} was considered to be equal to M_{rBC} because we assume that the background BC is zero since the atmospheric lifetime of BC is known to be of a few days (Park et al., 2005). By contrast the CO lifetime is estimated to be several days (Bey et al., 2001).

The mass absorption cross-section of rBC (MAC_{rBC}) was determined as

$$MAC_{rBC} = \frac{\sigma_{abs,880}}{M_{rBC}}. \quad (4)$$

M_{rBC} values below the 5th and above the 95th percentile were filtered before MAC_{rBC} calculations to reduce the influence of outliers in statistical analyses. In addition, we filtered out periods when dust was sampled at PDM for the calculation of MAC_{rBC} since Yus-Díez et al. (2021) observed significant biases in the multiple-scattering correction of the Aethalometer AE33 during such events.

The light-absorption enhancement factor E_{abs} can be determined as the MAC_{rBC} value normalized by a reference value for pure, uncoated (bare) rBC:

$$E_{abs} = \frac{MAC_{rBC}}{MAC_{bare,rBC}}. \quad (5)$$

Three different methods are generally used to estimate $MAC_{bare,rBC}$: the first one is to remove the coating of BC with a thermodenuder and measure the corresponding absorption (Cappa et al., 2012; Healy et al., 2015; Yuan et al., 2021); the second one is to extrapolate measurements of MAC_{rBC} as a function of the measured rBC mixing ratio (Cappa et al., 2019; Yuan et al., 2021); the third one consists in calculating $MAC_{bare,rBC}$ from the measured rBC size distribution using Mie's theory and the mean geometric rBC diameter (Zanatta et al., 2018; Liu et al., 2017; see Fig. S4 in the Supplement). Here we used the latter method by assuming a rBC refractive index of $1.95–0.79i$ at $\lambda = 880$ nm (Bond and Bergstrom, 2006). The calculation of $MAC_{bare,rBC}$ using Mie's theory assumes a simplified spherical assumption of rBC morphology. However rBC may exhibit complex morphologies whose optical behavior is imperfectly predicted by Mie's theory, introducing a bias into the retrieved $MAC_{bare,rBC}$ (Saleh et al., 2016). It might be considered that Mie's theory is suitable for estimating the absorption of highly aged rBC, which exhibits an internally mixed core–shell structure. China et al. (2015) used this method to calculate the E_{abs} of rBC in a high-altitude site of the Azores because the large majority (70 %) of these long-range-transported particles were found to be highly compacted. Several studies found that Mie's scattering model captures basic optical properties of BC in biomass burning plumes (Liu et al., 2017; Denjean et al., 2020). Zanatta et al. (2018) calculated MAC_{rBC} values of heavily coated rBC particles from the Arctic region using

Mie's theory and found results consistent with direct measurements. In addition to the morphology, the $MAC_{bare,rBC}$ calculation is also very sensitive to the refractive index of rBC core (Sorensen et al., 2018). F. Liu et al. (2020) summarized the changes in MAC values induced by the use of different refractive indexes. They reported deviations of −7 % to −35 % from the MAC_{BC} value of 7.5 $m^2\,g^{-1}$ recommended by Bond and Bergstrom (2006).

Time periods with high humidity (95 %) or precipitation were filtered before analysis to avoid artifacts in the sampling inlet. Under precipitation some water droplets may indeed enter in the aerosol inlet and change both the inlet cutoff diameter and the measured aerosol size distribution. This would bias all the measured aerosol properties. We also filtered periods where hourly CO concentrations exceeded 200 ppb in order to exclude local pollution events, e.g., due to snow removal of the touristic platform.

All aerosol and gas measurements were converted to standard temperature and pressure (273.15 K and 1013.25 hPa).

2.4 Identification of air mass origins

HYSPLIT (Stein et al., 2015) was used to calculate air masses back trajectories. This model uses 3-hourly atmospheric data from the Global Data Assimilation System (GDAS) of the National Centers for Environmental Prediction (NCEP) at a 1° × 1° spatial resolution. More information can be found at https://www.ready.noaa.gov/index.php (last access: 23 January 2024). A back trajectory was run at 12:00 UTC for each day, going back 72 h, for the 2 years of the campaign. Precipitation rates along the back trajectories were also computed from the HYSPLIT calculations in order to classify days when the air masses arriving at PDM encountered precipitation or not in the past 72 h.

To discriminate between FT- and PBL-influenced air masses (hereafter referred as PBL/FT conditions), we followed a methodology proposed initially by Griffiths et al. (2014), assuming that the diurnal radon increase, which is typically observed at mountain sites during the daytime, is the result of transport of PBL air by thermal anabatic winds up to the summits. The method first consists in ranking the days of the sampling period by decreasing anabatic influence (details in the Supplement and in Griffiths et al., 2014). A threshold rank (here 282; see Fig. S5 and the associated Text S3 in the Supplement) can then be determined to separate days with or without anabatic influence in the daytime.

In our study, it was necessary to select the observation hours strongly influenced by the boundary layer. To do this, we selected the first 200 anabatic days in the ranking and, from these days, all the hours when radon activity was greater than the median value for the current day.

We also needed an ensemble of observation hours with minimum influence of the PBL. In the latter case, we selected hours during the non-anabatic days (i.e., ranked after 282) with radon activity below the median value for the current day.

3 Results

3.1 Meteorology and air mass classification

In the following, seasons are defined as follows: winter (December, January, February), spring (March, April, May), summer (June, July, August) and autumn (September, October, November). The meteorological conditions at PDM during the campaign are described in Fig. S6 and the associated Text S4 in the Supplement.

The backward trajectories performed with the HYSPLIT model for 72 h time periods were assigned to six geographical zones, according to the position of their starting point (shown in Fig. 2): Northwest Europe, Continental Europe, Mediterranean Africa, Atlantic Spain, North Atlantic and Local (within a circular zone of 100 km radius around PDM). The transport to PDM was generally from the west or south, i.e., from the North Atlantic and Atlantic Spain zones. It should also be noted that 99 % of all atmospheric backward trajectories modeled to PDM reveal long-range transport (> 100 km).

The analyses of the diurnal cycle of radon concentrations allowed us to determine the FT and PBL conditions prevailing at the site following the methodology presented in Sect. 2.4. Details on the statistical results can be found in Table S1 in the Supplement. Over the campaign, 1149 h was clearly identified as FT-influenced conditions, which represents 56 % of the total classified hours. In winter, FT and PBL conditions occurred roughly 74 % and 26 % of the analyzed time, respectively, against 48 % and 52 % for summer, respectively. These results are broadly in agreement with the previous study by Hulin et al. (2019) at PDM, which quantified around 47 % of the days as PBL-influenced over a 10-year period. The PBL conditions occurred mostly around 15:00 UTC (see Fig. S5), consistent with the dynamics at mountain sites where plain-to-mountain winds and along-valley winds become the strongest in the afternoon (Whiteman, 2000).

3.2 Aerosol optical properties and classification of aerosol types

Figure 3 presents daily time series and statistics of aerosol optical properties over the 2-year measurement period. The average SSA ± GSD (geometric standard deviation) were 0.94 ± 0.06, 0.94 ± 0.07 and 0.95 ± 0.08 at 450, 525 and 635 nm, respectively (Fig. 3a). These values are in the range of those observed at mountain sites in southern Europe (Bukowiecki et al., 2016; Laj et al., 2020; Pandolfi et al., 2014). The mean value ± GSD of $\sigma_{abs,880}$ was 0.27 ± 0.25 Mm^{-1} (Fig. 3b), which falls in the range of 0.14 to 1.23 Mm^{-1} obtained at Jungfraujoch and

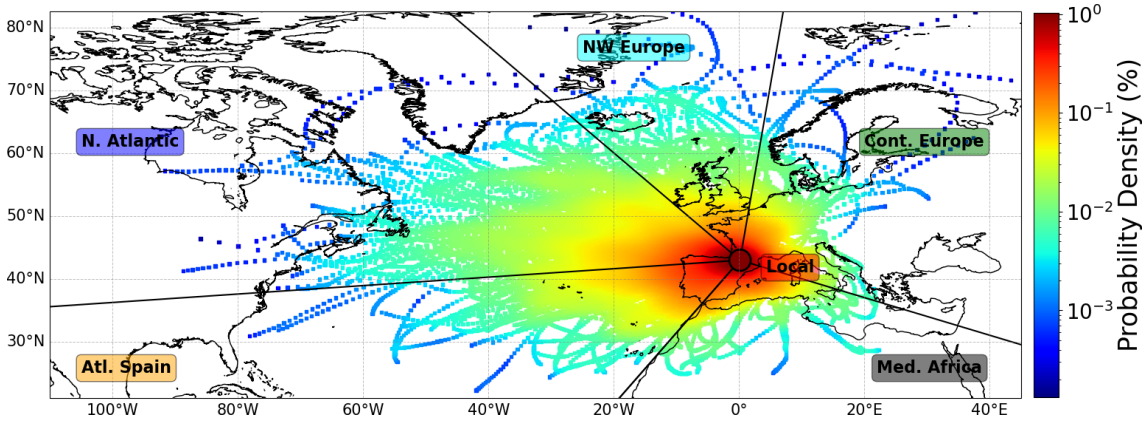

Figure 2. The 72 h back trajectories of air masses measured at PDM over the measurement period 2019–2020. Geographical boundaries of the sectors used to classify the air mass back trajectories are overlaid.

Montsec (Bukowiecki et al., 2016; Pandolfi et al., 2014). The average σ_{sca} ± GSD values were $15.5 \pm 16.1\,Mm^{-1}$, $13.4 \pm 13.9\,Mm^{-1}$ and $12.2 \pm 12.9\,Mm^{-1}$ at 450, 525 and 635 nm, respectively (Fig. 3c). These weak values of σ_{abs} and σ_{sca} can be explained by the remote mountain site type, where almost no aerosols are locally emitted. There was a clear seasonality of aerosol optical properties. SSA at the three wavelengths exhibited the lowest monthly mean values in spring–summer (0.94 ± 0.02 at $\lambda = 525$ nm) and the highest in autumn–winter (0.99 ± 0.01 at $\lambda = 525$ nm, as shown in Fig. 3a). Simultaneously, the highest monthly mean SAE values were observed in spring–summer (1.23 ± 0.70) and reached a minimum in the winter (-0.25 ± 0.16) (Fig. 3d). This anticorrelation suggests a higher fraction of absorbing and fine particles relative to purely scattering and coarse particles at PDM during the spring–summer. Interestingly different trends can be observed between the summer and spring seasons. During spring 2019 the decrease in SSA is correlated with a slight enhancement of $\sigma_{abs,880}$ (Fig. 3b) and a decrease in σ_{sca} at all wavelengths. In summer the increase in $\sigma_{abs,880}$ leads to values multiplied by a factor of 4, while both SSA and SAE remain rather constant. All these parameters combined indicate a similar dominant aerosol type reaching PDM but with a stronger contribution in summer. This noteworthy seasonality of aerosol optical properties has previously been observed at other high mountain sites in Europe (Andrews et al., 2011; Collaud Coen et al., 2011; Laj et al., 2020; Pandolfi et al., 2018). The higher concentration of small and absorbing particles in summer at PDM could be attributed to a higher anthropogenic BC influence favored by strong vertical mixing and a higher PBL height, a higher occurrence of wildfires emitting large amounts of BC and brown carbon (BrC), or a lower precipitation rate.

In order to investigate these different hypotheses, a classification of the dominant aerosol type sampled at PDM was performed using the spectral dependency of aerosol optical properties. Figure 4 shows AAE as a function of SAE, overlaid with the aerosol classification matrix from Cappa et al. (2016). Aerosols with the highest SSA values (violet points) tend to fall on the left-hand side of the plot with SAE values below 0, indicative of large particles such as marine sea salt, continental dust or highly processed/coated particles. The presence of large marine and dust aerosols is in line with backward trajectories showing a dominant origin of air masses coming from the Atlantic Ocean and Iberian Peninsula as far as north Africa (e.g., Fig. 2). Dust being a strong light absorber, it is expected to lower the mean aerosol SSA. However Fig. 4 shows that SSA values for dust-dominated aerosol (classified as having AAE values above 2) are quite similar to those for remote marine aerosol (classified as having AAE values below 1). Although Europe frequently experiences African dust events (Denjean et al., 2016; Dumont et al., 2023), our results indicate that these dust events were not absorbing enough to substantially lower the aerosol SSA at PDM. This is supported by previous estimates of SSA ranging between 0.90 and 1.00 for dust particles transported in the Mediterranean region (Mallet et al., 2013; Denjean et al., 2016).

There a natural clustering of the most light-absorbing aerosols with SSA < 0.9 (pink to yellow points) in the middle of the plot, with sections on the lower side with AAE between 0.5 and 1.5, which Cappa et al. (2016) defined as the sections dominated by BC or a mix of BC and large particles. The success of aerosol classification schemes is largely dependent on uncertainties in AAE attribution for each aerosol species. Although AAE = 1 is often considered to be BC such as that in the classification by Cappa et al. (2016), observational and numerical estimates show a wide range of BC AAE from 0.6 to 1.3 (Kirchstetter et al., 2004; Liu et al., 2018) due to the variation in BC core size, coating thickness, composition and morphology (Liu et al., 2018; Zhang et al., 2018). Therefore it is possible that the large range of AAE values observed for the most light-absorbing aerosols was

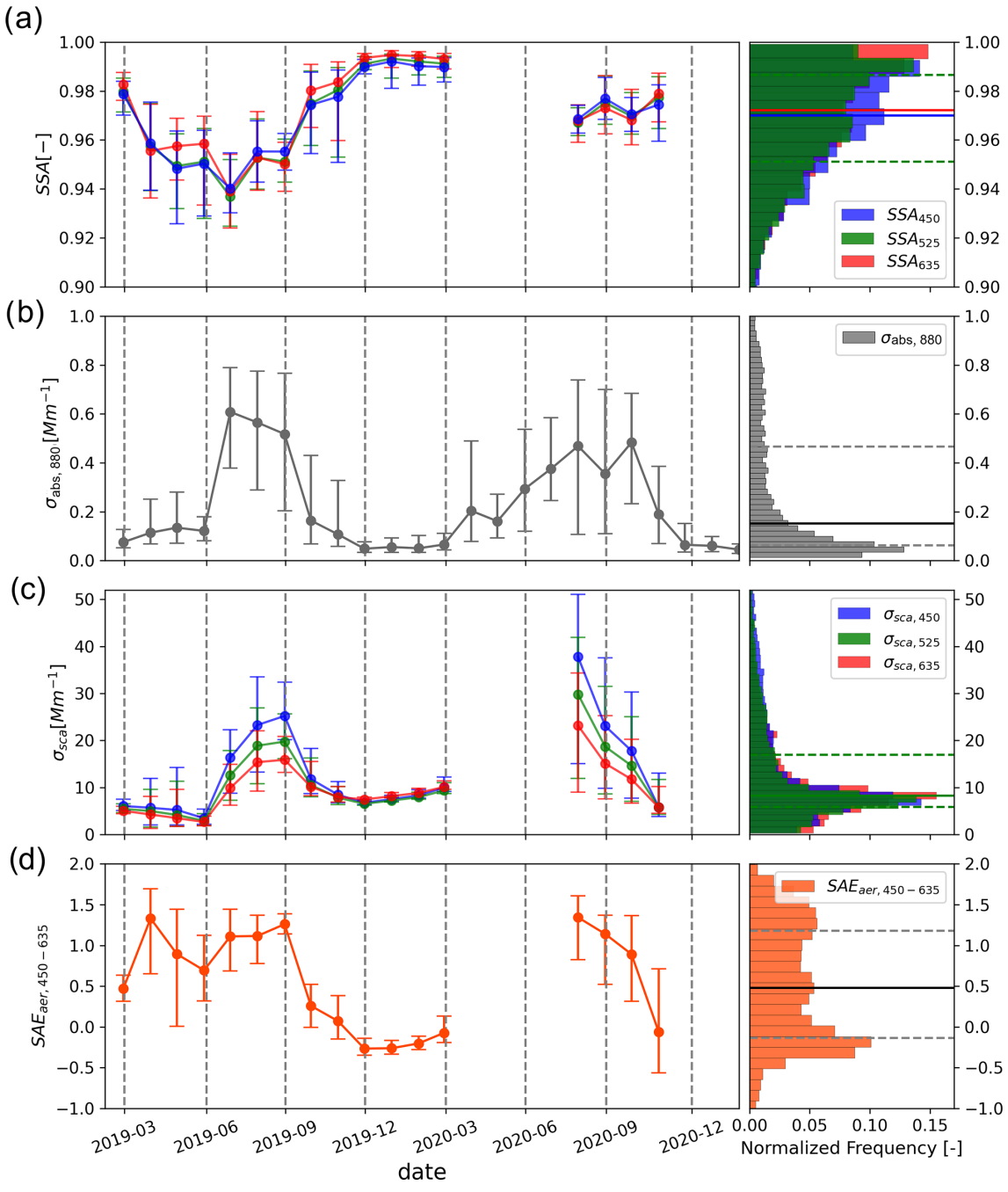

Figure 3. Time series (left) and statistical distributions (median and 25th and 75th percentiles, right) of aerosol optical properties measured at PDM in 2019–2020 with **(a)** single-scattering albedo at 450, 525 and 635 nm; **(b)** absorption coefficient at 880 nm; **(c)** scattering coefficients at 450, 525 and 635 nm; and **(d)** scattering Ångström exponent at 450–635 nm. The dots and bars on the time series represent the median and the 25th and 75th percentiles, respectively, with a monthly frequency. Histograms was computed using a 1 d time frequency. Vertical dashed lines represent the seasons' boundaries. The date format is year-month.

due to different microphysical and chemical properties of the BC sampled at PDM.

Interestingly almost none of the aerosols were classified as strong BrC and BC/BrC mixture (AAE and SAE values above 1.5), revealing a very low contribution of BrC to the aerosol absorption at PDM. An explanation for this could be the rapid BrC depletion within the first day of emission, by photobleaching or volatilization that has been observed in several studies (Forrister et al., 2015; Wong et al., 2019; Zeng et al., 2020). Altogether these results suggest that BC was the

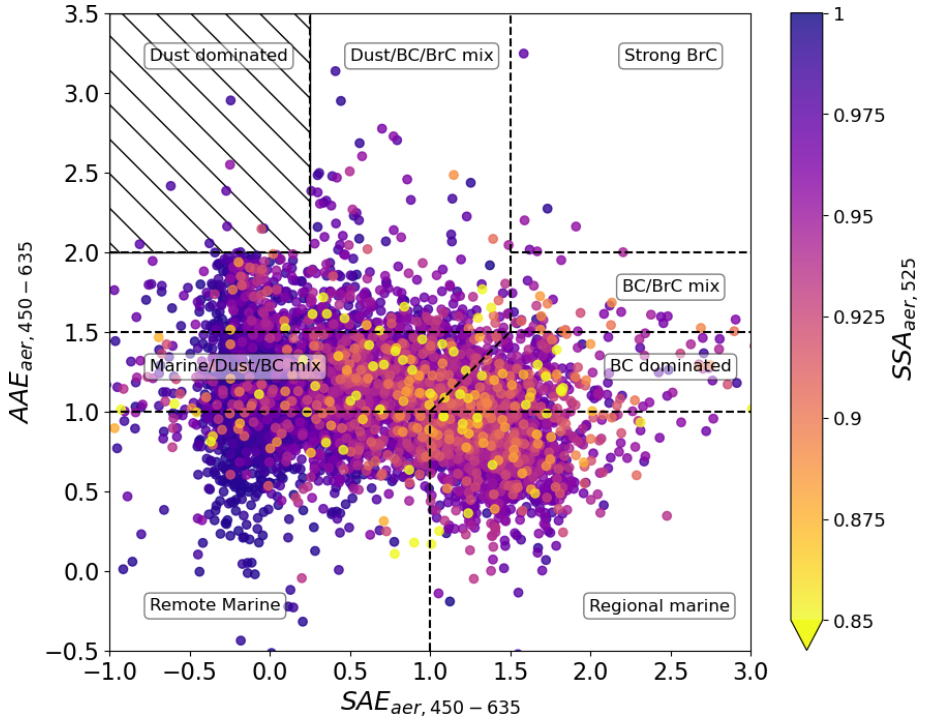

Figure 4. Hourly average aerosol absorption Ångström exponent vs. scattering Ångström exponent calculated at 450–635 nm and colored as a function of the single-scattering albedo at 525 nm. The classification of aerosol type by Cappa et al. (2016) is also shown. The points in the dashed zone, representing dust events, were filtered before analyses of BC properties to avoid artifacts in the calculation of MAC_{rBC}.

predominant absorption component of aerosols at PDM and controlled the variation in SSA throughout the 2 observation years.

3.3 rBC sources and properties

3.3.1 rBC mass concentration

Figure 5 shows the time series of the microphysical and optical properties of rBC. The mean M_{rBC}, shown in Fig. 5a, was 34.8 ± 35.7 (mean $\pm$ SD) ng m^{-3}, which is a typical level for remote mountain sites. For instance, Sun et al. (2021) observed M_{eBC} around 20 ng m^{-3} from 9 years of measurements with a multi-angle absorption photometer (MAAP; model 5012, Thermo Scientific) at the Schneefernerhaus station, Zugspitze, Germany (2671 m a.s.l.). Motos et al. (2020) measured M_{rBC} around 9 ng m^{-3} in summer at Jungfraujoch, Switzerland (3580 m a.s.l.). rBC represented around $7\,\% \pm 5\,\%$ of the total aerosol number concentration measured by the SMPS over the campaign. An increase in the rBC number fraction by a factor of 2.5 was found in summer ($9\,\% \pm 5\,\%$) compared to winter ($4\,\% \pm 3\,\%$). Simultaneously, $\sigma_{abs,880}$ increased by a factor of 4 between winter and summer. Thus, this confirms that rBC contributed to a significant part of the aerosol absorption at PDM.

3.3.2 rBC emission sources

Figure 6 shows bivariate polar plots obtained by combining wind analysis and M_{rBC} with a 1 h time resolution in winter and summer. The densities of M_{rBC} data weighted by M_{rBC} values and normalized by the maximum density of M_{rBC} were plotted as a function of the wind direction and speed. The darkest areas of the wind pattern are those where the highest M_{rBC} was measured with a high occurrence, whereas the lightest zones exhibit the lowest measured M_{rBC} and/or a low occurrence of measurements. Note that locally emitted pollution at the measurement station was filtered before the analysis, limiting local M_{rBC} contributions emitted from the PDM station (e.g., Sect. 2.3).

In summer, the highest M_{rBC} values were mainly associated with moderate wind speeds (above 5 m s^{-1}) and from the west and southwest, suggesting a dominant regional transport (Fig. 6a). By contrast in winter (Fig. 6b), the highest M_{rBC} mainly occurred under more static atmospheric conditions (i.e., for wind speeds below 5 m s^{-1}) and with no evident wind direction dependency. These results suggest that local-scale emissions could be a major contributor to M_{rBC} in winter, unlike in summer. Further discussion on the role of PBL influence on M_{rBC} is given in Sect. 3.4.2.

The $\Delta M_{rBC}/\Delta CO$ emission ratio, presented in Fig. 5b, shows a wide range of values from 0 to 10 ng m^{-3} ppbv^{-1}, with a mean value of 1.93 ± 2.12 ng m^{-3} ppbv^{-1}. Sum-

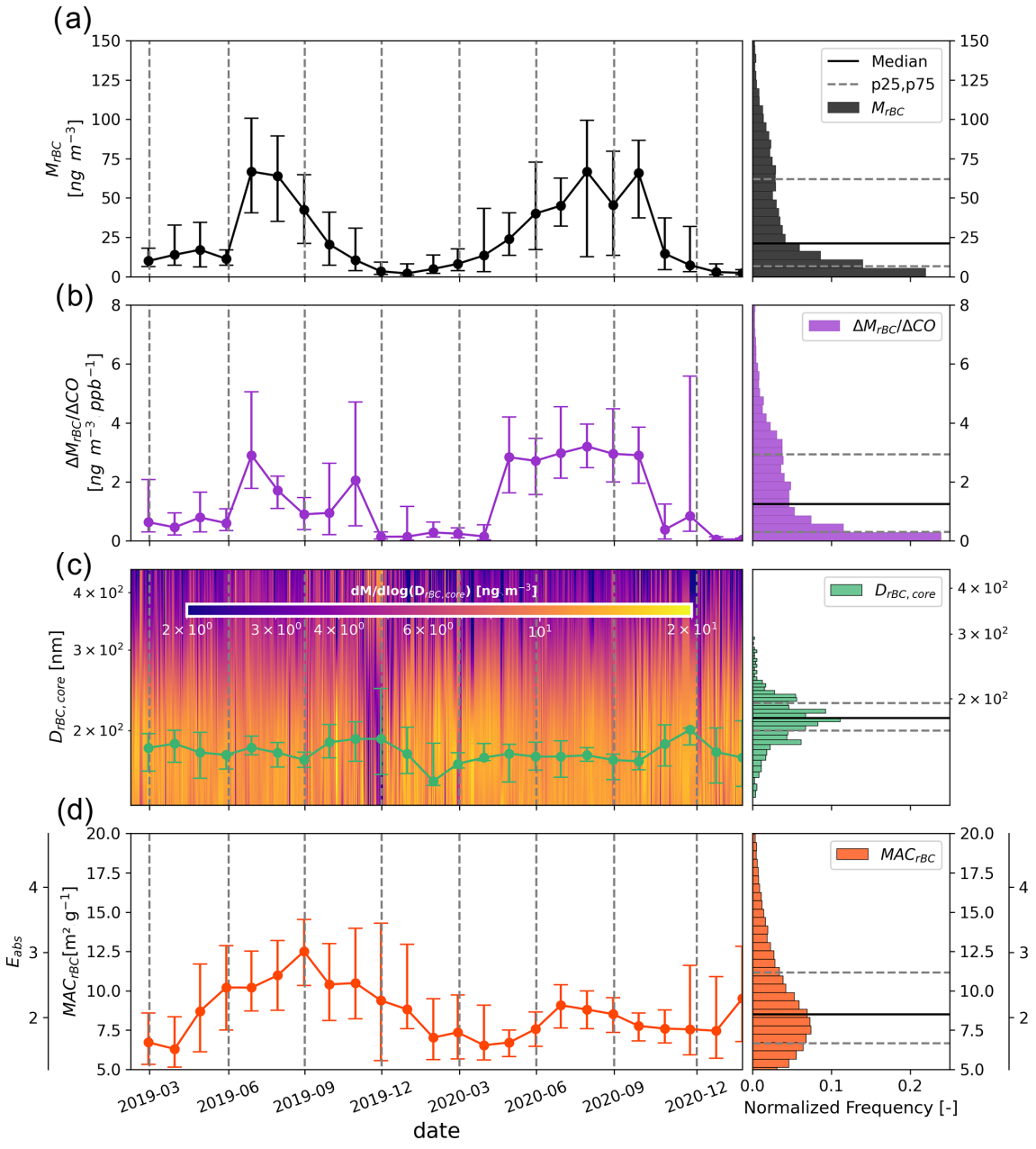

Figure 5. Time series (left) and statistical distributions (median and 25th and 75th percentiles, right) of rBC properties measured at PDM in 2019–2020: **(a)** rBC mass concentration, **(b)** $\Delta M_{\mathrm{rBC}}/\Delta\mathrm{CO}$ emission ratio, **(c)** rBC core mass size distribution with geometric diameter in solid green line, and **(d)** rBC mass absorption cross-section and absorption enhancement at 880 nm. The dots and bars on the time series represent the median and the 25th and 75th percentiles, respectively, with a monthly frequency. Histograms was computed using a 1 d time frequency, as well as the colored background of the rBC core size distribution. Vertical dashed lines represent the seasons' boundaries. The date format is year-month.

mer ratios were generally higher than winter emission ratios, which could reflect either lower rBC scavenging during transport or different emission sources of rBC between seasons. Indeed, the $\Delta M_{\mathrm{rBC}}/\Delta\mathrm{CO}$ emission ratio varies as a function of fuel types, combustion efficiencies and wet deposition by precipitation (Baumgardner et al., 2002; Taylor et al., 2014). This explains the high diversity of $\Delta M_{\mathrm{rBC}}/\Delta\mathrm{CO}$ emission ratios obtained in the literature worldwide, going from 0.5 ng m^{-3} ppbv^{-1} at Jungfraujoch, Switzerland (Liu et al., 2010), to 9 ng m^{-3} ppbv^{-1} in a biomass burning plume above the Texas region during the TexAQS 2006 campaign, USA (Spackman et al., 2010), if only studies using SP2 measurements are considered. Overall $\Delta M_{\mathrm{rBC}}/\Delta\mathrm{CO}$ from fossil fuel tends to exhibit lower values

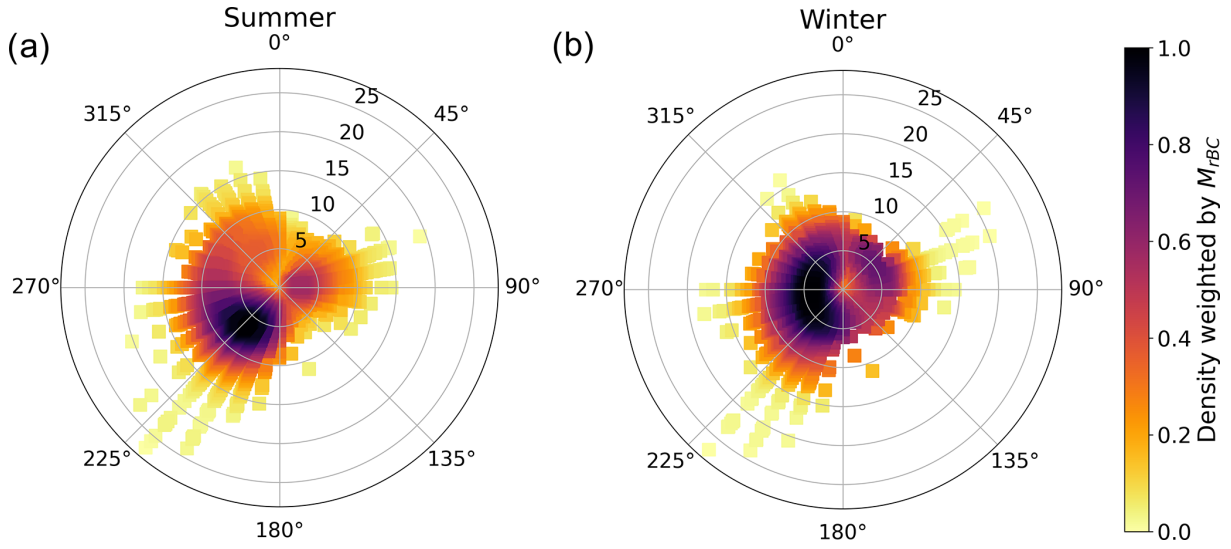

Figure 6. Bivariate polar plots of the density of M_{rBC}, weighted by M_{rBC} values as a function of the wind direction and speed in **(a)** summer and **(b)** winter. The color scale shows the M_{rBC} density data weighted by M_{rBC}. The radial scale shows the wind speed, which increases from the center of the plot radially outwards. Both plots use hourly data. The weighted densities were normalized by their maxima.

than that from biomass combustion (Guo et al., 2017; Pan et al., 2011; Zhu et al., 2019). To our knowledge the only available $\Delta M_{\mathrm{rBC}}/\Delta\mathrm{CO}$ measurements in Europe were performed during airborne measurements in the Cabauw industrial region, the Netherlands, by McMeeking et al. (2010), who found very low values of around $0.8\,\mathrm{ng\,m^{-3}\,ppbv^{-1}}$. The high time variability in $\Delta M_{\mathrm{rBC}}/\Delta\mathrm{CO}$ reflects important differences concerning the scavenging processes impacting BC and/or the relative contribution of biomass burning and fossil fuel emissions in the production of BC measured at PDM. These two different factors will be addressed in Sect. 3.4.

3.3.3 rBC mass size distribution

The rBC mass median core size diameter ($D_{\mathrm{rBC,core}}$) was quite constant during the campaign with a mean geometric diameter of 179 ± 28 nm (Fig. 5c). An exception occurred in early December 2019, when we detected the presence of large rBC particles with $D_{\mathrm{rBC,core}}$ around 400 nm. However observations during this period may be the results of measurement uncertainties due to too low an M_{rBC} (less than $10\,\mathrm{ng\,m^{-3}}$). The $D_{\mathrm{rBC,core}}$ values obtained at PDM are generally comparable to $D_{\mathrm{rBC,core}}$, which has been reported ranging from 180 to 225 nm for well-aged background rBC (Liu et al., 2010; McMeeking et al., 2010; Schwarz et al., 2010; Shiraiwa et al., 2008). However, our values are slightly higher than previous observations at Jungfraujoch by Motos et al. (2020), who reported $D_{\mathrm{rBC,core}}$ ranging from 130 to 150 nm in summer and winter. Instead of fitting the SP2 observations with multimodal individual lognormal modes (e.g., Sect. 2.2.2), Motos et al. (2020) only took into account rBC particles with $D_{\mathrm{rBC,core}} > 50$ nm (the lower detection limit of their SP2 version), which may bias the estimated SP2 mode of $D_{\mathrm{rBC,core}}$ (Tinorua et al., 2024).

3.3.4 rBC absorption

The ambient $\mathrm{MAC_{rBC}}$ was around $9.2 \pm 3.7\,\mathrm{m^2\,g^{-1}}$ at $\lambda = 880$ nm (Fig. 5d). Several studies have previously reported $\mathrm{MAC_{BC}}$ values between 8.9 and $13.1\,\mathrm{m^2\,g^{-1}}$ for measurements at $\lambda = 637$ nm in European mountain stations (Pandolfi et al., 2014; Yus-Díez et al., 2022; Zanatta et al., 2016). By using an AAE of unity, these values can be converted to $\mathrm{MAC_{BC}}$ between 6.4 and $9.5\,\mathrm{m^2\,g^{-1}}$ at $\lambda = 880$ nm. These studies used different measurement techniques, analysis methods and correction factors from ours for estimating $\mathrm{MAC_{BC}}$, which makes difficult the comparison of $\mathrm{MAC_{rBC}}$ derived from different instruments. Pandolfi et al. (2014) performed a linear regression between $\sigma_{\mathrm{abs},637}$ measured by a MAAP (multi-angle absorption photometer) and daily M_{EC} values from off-line filter-based measurements by a Sunset OCEC analyzer. Yus-Díez et al. (2022) and Zanatta et al. (2016) retrieved $\mathrm{MAC_{BC}}$ with these instruments by calculating the ratio between the two parameters instead of a linear regression. Because of the absence of a standard method for quantifying M_{BC}, the absolute uncertainties in the $\mathrm{MAC_{BC}}$ obtained in the literature are very high, ranging from ±29 % to ±63 % (Zanatta et al., 2016).

In terms of seasonality we found systematically higher values of $\mathrm{MAC_{rBC}}$ in summer (monthly mean ± SD of $10.3 \pm 3.3\,\mathrm{m^2\,g^{-1}}$) compared to winter ($8.3 \pm 3.8\,\mathrm{m^2\,g^{-1}}$). A similar seasonal pattern was observed in Europe at Puy de Dôme (Zanatta et al., 2016, central France) and at Jungfrau-

joch (Swiss Alps) mountain sites (Motos et al., 2020). An opposite trend was observed at mountain sites affected by strong precipitation during monsoon such as the Tibetan Plateau and Himalayan regions, where both MAC_{BC} and M_{BC} exhibit maximum values in winter or autumn (Zhao et al., 2017; Srivastava et al., 2022). The same seasonal pattern with elevated values in winter/autumn compared to summer/spring was observed at several rural and urban sites in the PBL, which was attributed to greater emissions from residential heating combined with a lower PBL height (Zanatta et al., 2016; Kanaya et al., 2016; Yttri et al., 2007). However maximum MAC_{BC} and M_{BC} in the PBL during cold periods are not a recurring observation even for the same measurement site. For instance Sun et al. (2022) showed that in Beijing (China), due to the reduction in some predominant BC sources in winter following environmental policies, the annual cycle of M_{BC} changed over the years between 2012 and 2020.

Variations in MAC_{rBC} may exist for different reasons. We first address the question of whether the MAC_{rBC} depends on $D_{rBC,core}$ in Fig. S7 in the Supplement. There was no clear correlation between MAC_{rBC} and $D_{rBC,core}$, which indicates that the variation in BC size was not the cause of the MAC_{rBC} variability. This is because $D_{rBC,core}$ only varied within a relatively narrow range (the 25th and 75th percentiles around 164 and 195 nm) during the campaign. The observed MAC_{rBC} values were converted to equivalent E_{abs} by dividing them by a reference MAC for pure, uncoated BC ($MAC_{bare,BC}$). While values of $MAC_{bare,BC}$ are reported in the literature, estimation of campaign-specific $MAC_{bare,BC}$ allows for more robust determination of E_{abs} than using values from the literature since $MAC_{bare,BC}$ is dependent on the size of uncoated BC (Bond and Bergstrom, 2006; Adachi et al., 2007, 2010; Adachi and Buseck, 2013; Cappa et al., 2012). Here the mean $MAC_{bare,BC}$ was $4.15\,m^2\,g^{-1}$, with values ranging from 3.90 to $4.37\,m^2\,g^{-1}$ considering the standard deviation of the mean $D_{rBC,core}$, which is in reasonable agreement with literature assessments (F. Liu et al., 2020).

The E_{abs} values relative to $MAC_{bare,BC} = 4.15\,m^2\,g^{-1}$ at $\lambda = 880$ nm were significantly greater than unity, with a mean value of 2.2 ± 0.9 (Fig. 5d). Given the remote mountain location and presumable distance from fresh rBC sources, rBC particles reaching PDM may have undergone aging and have gained a consistent coating. Previous studies found an absorption enhancement of BC due to its coating with the aging time (Yus-Díez et al., 2022; Sedlacek et al., 2022; Peng et al., 2016). The most likely cause of the strong E_{abs} at PDM is a lensing effect due to the internal mixing of rBC with other particles that drives MAC_{rBC} variability, though we cannot eliminate changes in rBC morphology that can result from coating onto rBC. There was a significant seasonal trend in E_{abs} with higher values observed in summer, indicating that rBC reaching the PDM station has undergone longer aging processes during this season. These results are consistent with the measurements of Motos et al. (2020) at Jungfraujoch, which also indicated a strong seasonality in the rBC mixing state with larger coating in summer.

Figure 7 further shows the diurnal variation in E_{abs} for every season. There was a notable opposite diurnal profile between seasons for E_{abs}, with midday showing a minimum of around 1.7 in winter and a maximum of around 2.9 in summer. Spring and autumn showed intermediate patterns with less regular E_{abs} throughout the day. These observations suggest that different sources and/or processes drove the seasonal contrast in rBC properties. Nonetheless, it cannot be ruled out that some of the variability in MAC_{rBC} (and E_{abs}) can be explained by the use of a fixed multiple-scattering correction applied to calculate σ_{abs}, since this parameter has been shown to vary as a function of time and atmospheric conditions (Yus-Díez et al., 2021). The following section aims to investigate potential drivers of E_{abs} variations, including rBC wet scavenging, dominant rBC sources and transport pathways. Particular attention will be paid to winter and summer because these seasons differ greatly, whereas spring and autumn behaviors appear intermediate.

3.4 Investigation of factors influencing rBC properties

3.4.1 The impact of wet scavenging on rBC properties

We first investigated whether E_{abs} was modulated by a size-dependent rBC wet scavenging process during precipitation along the transport pathway of rBC-containing particles. This hypothesis is based on the fact that the removal of particles is favored for the largest and thickly coated rBC because the activation of aerosols into cloud droplets is predominantly controlled by the particle size (Moteki et al., 2012; Mori et al., 2021; Ohata et al., 2016; Zhang et al., 2021). The wet removal of rBC was investigated by performing a cluster analysis using $\Delta M_{rBC}/\Delta CO$ data for which precipitation occurred or did not along 72 h back trajectories computed by the HYSPLIT model. In order to decrease the influence of the difference sources on $\Delta M_{rBC}/\Delta CO$ compared to the effect of wet scavenging, periods for which the site was under PBL influence were filtered.

Figure 8a shows a median $\Delta M_{rBC}/\Delta CO$ of $0.7\,ng\,m^{-3}\,ppbv^{-1}$ for air masses affected by precipitation, against $2.1\,ng\,m^{-3}\,ppbv^{-1}$ without precipitation during the transport of the air masses. The reduction in $\Delta M_{rBC}/\Delta CO$ by a factor of 3 suggests that a significant removal process of rBC from the precipitation occurred along the transport pathway, apart from vertical transport from the PBL. As a reminder, time periods when PDM was under precipitation or humidity $> 95\,\%$ have been filtered before the analysis. This result is confirmed by the dependence of $\Delta M_{rBC}/\Delta CO$ on RH in Fig. 8b, where a sudden decline in $\Delta M_{rBC}/\Delta CO$ appeared for the highest RH $> 80\,\%$, going from a median $\Delta M_{rBC}/\Delta CO$ of between 2.0 and $2.4\,ng\,m^{-3}\,ppbv^{-1}$ for RH $< 80\,\%$ to a median $\Delta M_{rBC}/\Delta CO$ of $\sim 0.4\,ng\,m^{-3}\,ppbv^{-1}$ above 80 % RH. This

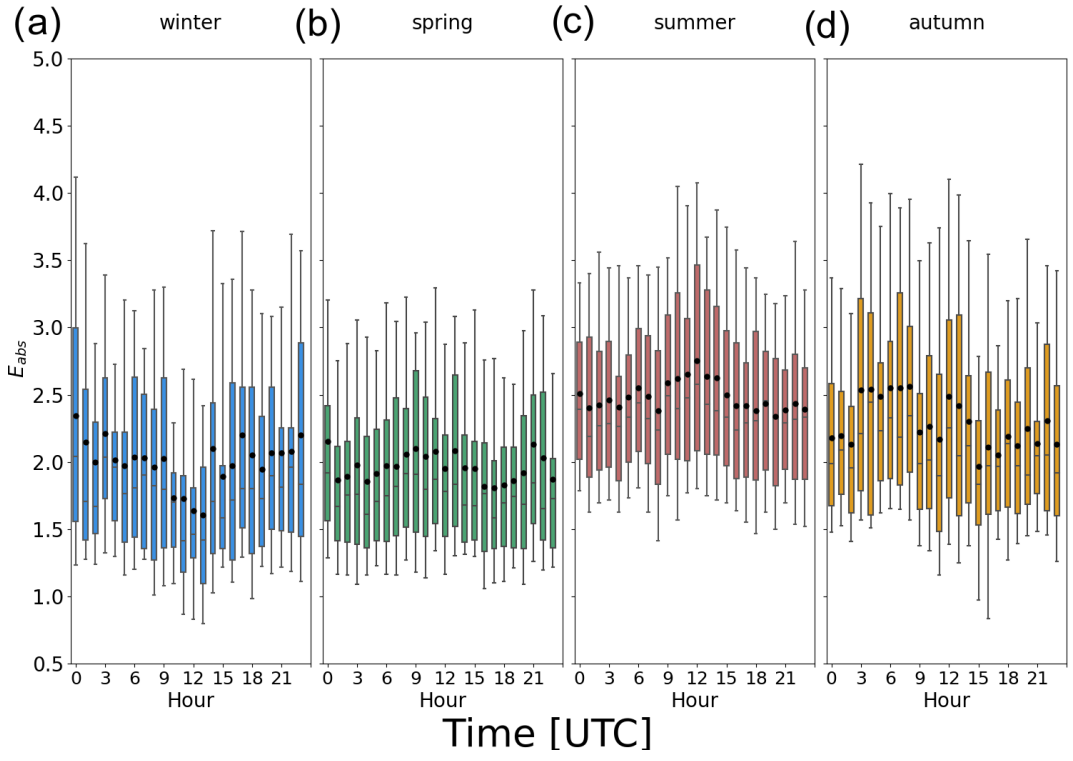

Figure 7. Diurnal cycles of E_{abs} for each season during the 2019–2020 period. Seasons are defined as follows: winter (December, January, February), spring (March, April, May), summer (June, July, August) and autumn (September, October, November). Boxes, lines, black dots and whiskers indicate the 25th percentile and 75th percentile, median, mean, and 10th percentile and 90th percentile, respectively.

result of high rBC removal by wet deposition is in line with measurements performed in regions at similar altitudes, such as Puy de Dôme, Mt. Tianjing and Mt. Sonnblick, where wet deposition represents 30 % to 70 % of the BC removing processes in the troposphere (Yang et al., 2019). Figure 8c and d show in contrast little influence of precipitation and RH on the rBC absorption enhancement, with a constant median E_{abs} value of around ~ 2.1.

To better understand the negligible impact of rBC wet scavenging on MAC_{rBC}, we compared the measured rBC core size distribution of air masses affected or not affected by precipitation during their transport and under high-RH conditions or not (Fig. 9). A 2-fold-lower M_{rBC} in precipitation conditions compared to that without precipitation provides additional evidence for the dominant role of wet scavenging for rBC. The same result appeared when comparing rBC core size distribution under wet or dry conditions. However no significant change in the mean rBC core diameter was noticed between wet and dry conditions (mean $D_{rBC,core}$ of 177 and 182 nm, respectively), as well as in the presence of precipitation during the transport of rBC or not (mean $D_{rBC,core}$ of 178 and 185 nm, respectively).

This result contrasts with previous studies conducted in the FT showing a decrease in rBC size due to wet scavenging (Kondo et al., 2016; Moteki et al., 2012; Taylor et al., 2014; D. Liu et al., 2020). For example, Kondo et al. (2016) found a

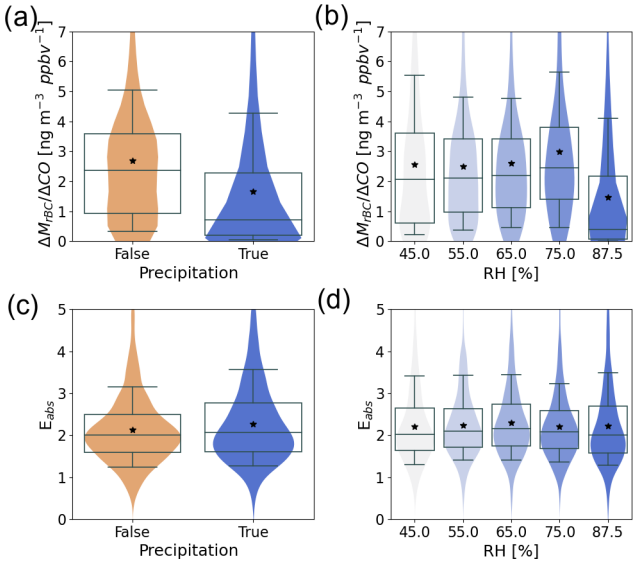

Figure 8. $\Delta M_{rBC}/\Delta CO$ emission ratio and E_{abs} vs. **(a, c)** precipitation along the air mass back trajectory calculated with the HYSPLIT model and **(b, d)** relative humidity measured at PDM. Violin plots represent the probability density function of each parameter. Features of the boxplots are defined in the same way as in Fig. 7. PBL conditions were filtered before analysis.

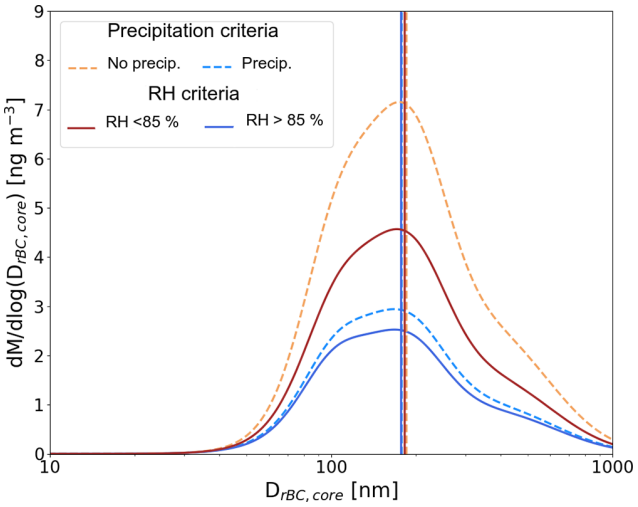

Figure 9. Mass size distributions of the rBC core measured by the SP2 as a function of the presence or absence of precipitation along the path of air masses arriving at PDM and whether the relative humidity was over 85 % or not. Vertical lines show the geometric mean rBC core diameter colored by the criteria described in the legend.

change in $D_{\mathrm{rBC,core}}$ between 13 and 20 nm depending on the season, while D. Liu et al. (2020) and Moteki et al. (2012) measured rBC cores $\sim$ 32 nm lower in air masses affected by wet removal. The insignificant effect of wet scavenging on the modal diameter of rBC core size distribution could be explained by the size of the rBC core sampled at PDM, which was higher than the one described in these studies. At the Jungfraujoch Hoyle et al. (2016) evidenced a threshold diameter of around 90 nm above which a particle is activated into a droplet upon cloud formation. The majority of rBC sampled at PDM exhibited $D_{\mathrm{rBC,core}}$ values above this critical diameter. In addition droplet activation of an aerosol particle occurs when the supersaturation of the surrounding water vapor exceeds a critical value of supersaturation. Thus, it is not likely for freshly emitted BC particles to act as cloud condensation nuclei due to their hydrophobic nature unless the water vapor supersaturation is higher than 2 % (Wittbom et al., 2014), far beyond the actual supersaturation (0.1 %–0.6 %) in ambient air. Furthermore, the rBC wet removal by impaction is also a size-dependent process which could have been responsible for the removal of small rBC particles (Croft et al., 2010). However interstitial scavenging mostly affects particles smaller than 100 nm (Pierce et al., 2015), which have a very low presence at PDM (rBC mean diameter of 180 nm). As the ambient supersaturation varies depending on the environment, it is difficult to conclude whether the insensitivity of rBC size distribution and E_{abs} to precipitation occurrence was solely due to the presence of large rBC particles at the sampling site or to a high ambient supersaturation in the precipitating clouds. Further measurements of simultaneous rBC wet removal and effective supersaturation are needed to test all these assumptions.

3.4.2 The contrasting seasonal influence of FT and PBL on rBC properties

Figure 10 shows the rBC properties classified by FT and PBL conditions (methodology in Sect. 2.5) and by season. As explained in Sect. 3.3.2, the $\Delta M_{\mathrm{rBC}}/\Delta\mathrm{CO}$ ratio depends on the condition of combustion (fuel type, efficiency) and wet deposition by precipitation (Baumgardner et al., 2002; Taylor et al., 2014). We observed in Sect. 3.4.1 a large decrease in $\Delta M_{\mathrm{rBC}}/\Delta\mathrm{CO}$ when precipitation occurred during the transport of the air masses. In order to investigate the influence of rBC sources on rBC properties, precipitation events (air masses for which precipitation occurred along 72 h back trajectories) were removed in this section.

In winter, we measured higher M_{rBC} values and variability in PBL conditions (39.5, 30.0 and 105 ng m^{-3} for the median and 25th and 75th percentiles, respectively) compared to in FT conditions (33.5, 10.4 and 45.4 ng m^{-3} for the median and 25th and 75th percentiles, respectively) (Fig. 10a). Furthermore the diurnal cycle of M_{rBC} in winter PBL conditions showed an enhancement in the daytime (Fig. S8 in the Supplement). This trend is consistent with intrusions of pollutants transported from PBL sources through convective mixing. During the night, pollution from the surface is trapped by the low height of the PBL and cannot reach the PDM. At the same time, the cleaner air transported in the FT may contribute to the dilution of M_{rBC} at the PDM. The higher $\Delta M_{\mathrm{rBC}}/\Delta\mathrm{CO}$ in PBL conditions (2.5 ± 2.3 ng m^{-3} ppbv^{-1} for the mean $\pm$ SD) compared to in FT conditions (0.6 ± 0.1 ng m^{-3} ppbv^{-1} for the mean $\pm$ SD) may indicate additional sources from biomass combustion from the valley (Fig. 10b), which could be attributed to either residential wood heating or stubble burning, which is still a common practice in the Pyrenees (González-Olabarria et al., 2015). Figure 10c shows that PBL conditions were associated with lower E_{abs} values (1.5 ± 0.3 for the mean $\pm$ SD) compared to FT conditions (1.9 ± 0.4 for the mean $\pm$ SD). Therefore, E_{abs} was strongly modulated by atmospheric dynamics in winter.

During summer, vertical transport from the PBL occurred on about half of the days analyzed in this study. Surprisingly, the M_{rBC} did not vary between PBL and FT influence, with values of 75.4 ± 33.2 ng m^{-3} (mean $\pm$ SD) and 80.2 ± 46.6 ng m^{-3}, respectively, meaning that the thermally driven PBL injection did not significantly impact M_{rBC} measured at PDM (Fig. 10d). This contrasts with our winter observations and most previous surface measurements at mountain sites, where the daytime PBL development has been shown to enhance aerosol mass concentration (Herrmann et al., 2015; Motos et al., 2020). The summer M_{rBC} values at PDM are twice as high as those observed in winter, which indicates a massive additional re-

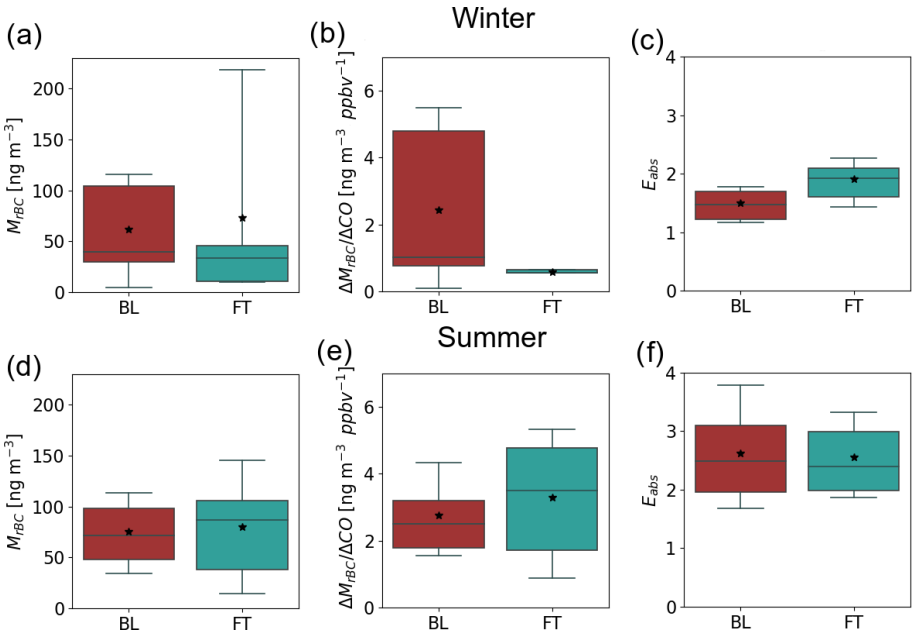

Figure 10. **(a)** rBC mass concentrations, **(b)** $\Delta M_{\mathrm{rBC}}/\Delta\mathrm{CO}$ emission ratio and **(c)** E_{abs} as a function of the predominant influence at PDM in winter. The same for summer is given in **(d)**, **(e)** and **(f)**. Red boxplots represent PBL conditions, and green boxplots represent FT conditions. Precipitation events were filtered before analyses.

gional transport of rBC in the FT and a lower contribution of rBC from PBL injection. $\Delta M_{\mathrm{rBC}}/\Delta\mathrm{CO}$ values in PBL and FT conditions were close to each other, with values of around $2.8 \pm 1.6\,\mathrm{ng\,m^{-3}\,ppbv^{-1}}$ (mean $\pm$ SD) and $3.3 \pm 1.7\,\mathrm{ng\,m^{-3}\,ppbv^{-1}}$, respectively (Fig. 10e). This result indicates that the FT exhibited a significant background load of rBC at the continental scale, thus limiting the relative influence of PBL injection on M_{rBC} during summer. The resulting E_{abs} was remarkably similar for PBL vs. FT air mass categories (Fig. 10f). The high rBC loading transported in the FT, coupled with the higher $\Delta M_{\mathrm{rBC}}/\Delta\mathrm{CO}$ observed in the summertime (Fig. 10d and e), could be due to a strong influence of biomass burning emissions on the background FT in Europe. The majority of trajectories reaching PDM in summer have crossed the Iberian Peninsula and, previously, north Africa and North America (Fig. S9 in the Supplement). In these regions large fire events frequently occur, which may explain the high concentrations of strongly absorbing rBC observed at PDM during summer. This hypothesis is supported by Petetin et al. (2018), who showed that biomass burning aerosol accounts for about 43 %–81 % of the CO concentration in the lower FT in summer using in situ airborne observations of CO from the IAGOS (In-service Aircraft for a Global Observing System) program. The ubiquitous presence of dilute biomass burning in the FT and its significant contribution to aerosol mass loading were also established using airborne measurements of ozone and precursor source tracers from the NASA Atmospheric Tomography Mission (Bourgeois et al., 2021; Schill et al., 2020). Additional measurements of the aerosol chemical composition and in particular of a tracer of biomass burning in the atmosphere such as levoglucosan should be performed at PDM to confirm this.

A question remains about the cause of the diurnal variation in E_{abs} in summer (Fig. 7c). As shown in Fig. 11, the E_{abs} increase was not temporally correlated with the wind direction change from west-southwest to south, as evidenced by the 2 h delay between the two events. Furthermore, while the E_{abs} increase occurs when $\Delta M_{\mathrm{rBC}}/\Delta\mathrm{CO}$ decreases, the E_{abs} drop in the afternoon was not accompanied by an increase in $\Delta M_{\mathrm{rBC}}/\Delta\mathrm{CO}$. Then an increase in E_{abs} in the morning was most likely due to further aging and the appearance of heavily coated rBC rather than a change in the rBC emission source. Several studies have highlighted the major role of photochemical processes and extensive secondary aerosol generation to promote the light-absorption enhancement of BC (Knox et al., 2009; Krasowsky et al., 2016; H. Liu et al., 2020; Wang et al., 2017; Xu et al., 2018; Yus-Díez et al., 2022). At PDM the enhanced E_{abs} at noon was accompanied by a shift of the aerosol accumulation mode towards larger sizes, which may be due to the condensation of gaseous species on aerosol particles (Fig. S10 in the Supplement). Simultaneously, a strong elevation of particle number concentration in the diameter range 10–30 nm can be observed, revealing new particle formation most likely produced by photochemical reactions at this time of day. It is thus possible that rBC particles became more coated via condensation of species produced by photochemical reactions at noon. How-

ever, it cannot be ruled out that the evolution of aerosol size distribution is a poor indicator of the rBC mixing state.

4 Summary and implications for climate models

Continuous 2-year measurements of refractory BC (rBC) properties and additional aerosol characteristics have been performed at the high-altitude mountain site Pic du Midi in the French Pyrenees. The classification of the dominant aerosol type using the spectral aerosol optical properties indicates that rBC is the predominant absorption component of aerosols at PDM and controls the variation in SSA throughout the 2 years. The lower SSA in summer (~ 0.93) than in winter (~ 0.97) is correlated with a higher rBC number fraction, whereas the influence of BrC and dust was found to be negligible.

One key parameter to constrain BC absorption and associated radiative forcing in climate models is the refractive index of BC, and in particular the resulting MAC_{BC}. It was not clear if BC at high-altitude mountain sites should have a thicker or thinner coating than in urban or plain sites or even should be coated at all. On the one hand, the longer BC lifetime and the low temperature in the free troposphere (FT) favor thicker coating due to enhanced condensation of low-volatility compounds in a colder environment. On the other hand, the low concentrations of particles and gaseous precursors in the FT may limit the coating processes. Our 2-year-long observations show that the overall net effect is a strong absorption enhancement with a mean E_{abs} value of 2.2 ± 0.9.

The value of $7.5\,m^2\,g^{-1}$ at $\lambda = 550\,nm$ of Bond and Bergstrom (2006) is the most common MAC_{BC} used in climate models. This recommendation was based on a compilation of experimental results for freshly generated BC at and near sources obtained earlier than the early 2000s. Nevertheless this value is largely under the MAC_{rBC} found in this study ($9.2\,m^2\,g^{-1}$ at $\lambda = 880\,nm$, which can be converted to $14.7\,m^2\,g^{-1}$ at $\lambda = 550\,nm$ assuming AAE = 1). The review by Moteki (2023) has also come to a similar conclusion. The reasons behind this bias should be better understood in the light of observations such as those provided in the present study.

This study has notably shown the high variability in rBC properties measured in a remote site, where rBC has undergone long-range transport and aging. Certain causes of the large variability in MAC_{rBC} have been eliminated and highlighted:

- Wet deposition is considered to be the main sink of BC, constraining its lifetime and size distribution and thus its atmospheric concentration and optical properties. Our direct $\Delta M_{rBC}/\Delta CO$ measurements show the important role of wet deposition as a sink of rBC with around 67 % removed in the atmosphere by precipitation. However, we found a negligible impact of the rBC wet removal process on both rBC size distribution and E_{abs}. This result may be due to the combination of large rBC particles reaching PDM ($D_{rBC,core}$ around 180 nm) and high critical supersaturation in precipitating clouds. The BC wet removal process was found to be one of the most misrepresented processes in the representation of BC in models (Textor et al., 2006; Yu et al., 2019), leading to overestimated BC tropospheric concentrations and lifetimes and, in fine, a higher simulated radiative forcing (Samset et al., 2014; Schwarz et al., 2013). Substantial controversial and ambiguous issues in the wet scavenging processes of BC are apparent in current studies (Yang et al., 2019). Our results suggest that a bulk-wet-deposition parameterization (which does not account for particle-size-dependent scavenging) could realistically represent the actual BC wet scavenging at this site.

- The rBC core was found to have a mean $D_{rBC,core}$ of 179 ± 28 nm, being reasonably independent of the season and day. There was no clear relationship between MAC_{rBC} and $D_{rBC,core}$, which indicates that the variation in rBC core size was not responsible for the MAC_{rBC} variability. Similar observations of the rBC core size distribution in the atmosphere provided observational evidence of the stable distribution, with a mode centered at around 200 nm approximately 1 d after emission (Liu et al., 2010; Schwarz et al., 2010; Shiraiwa et al., 2008). This self-similarity could greatly simplify the representation of MAC_{BC} in model simulations, since a description of the BC mixing state becomes the determinant factor of model performance when estimating BC optical properties and radiative forcing.

- Different timescales of air movements and atmospheric processes affect MAC_{rBC} throughout the year. MAC_{rBC} values were found to be higher in summer (geometric mean of $10.3\,m^2\,g^{-1}$), when the influence of regional-scale motions dominates the rBC load, than in winter (geometric mean of $8.3\,m^2\,g^{-1}$), when the influence of local-scale motions outweighs the rBC load. There are three possible explanations for this. (i) The plumes traveling in the FT tend to have a longer lifetime, providing sufficient time for rBC aging during transport. In winter this results in a strong diurnal variability in M_{rBC} (E_{abs}) with higher (lower) values in the middle of the day linked to the injection of rBC originating from the planetary boundary layer (PBL). However the aging timescale cannot be the only explanatory factor since thermally driven PBL injection did not significantly impact M_{rBC} and E_{abs} in summer and higher values have been observed in summer than in winter for similar FT conditions. (ii) The source of rBC emission was different between the winter and summer seasons. Combining $\Delta M_{rBC}/\Delta CO$ with air mass transport analysis, we observed additional sources from biomass burning in summertime, leading to higher M_{rBC} and E_{abs}. (iii)

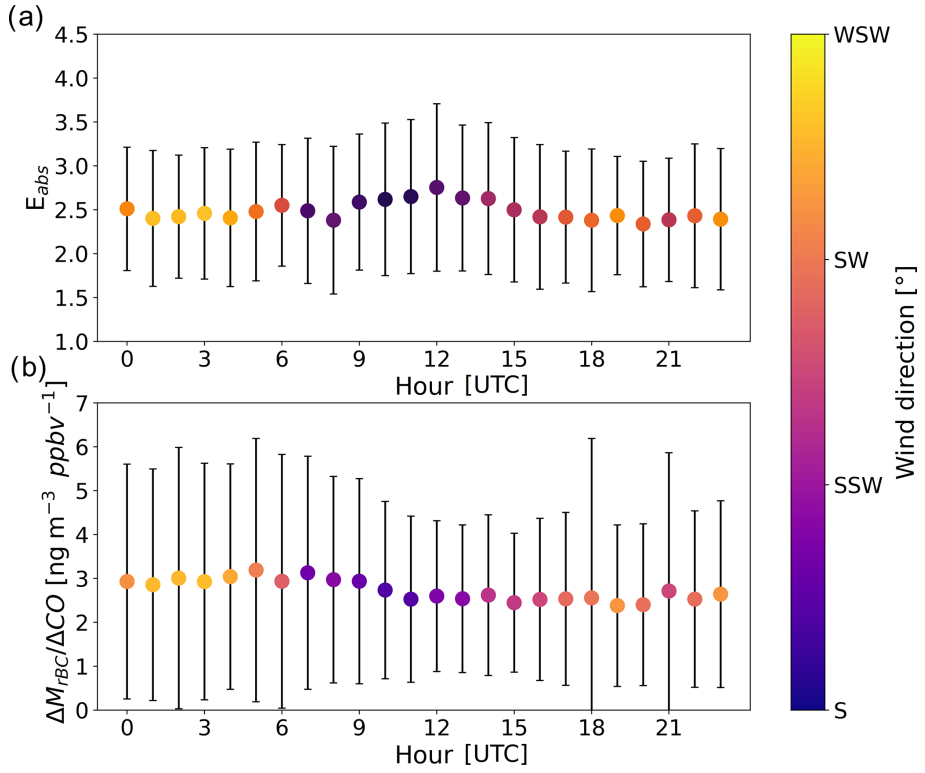

Figure 11. Hourly variation in **(a)** E_{abs} and **(b)** $\Delta M_{\mathrm{rBC}}/\Delta\mathrm{CO}$ values in summer. Dots represent mean values, and whiskers are 1 standard deviation. Dots are colored as a function of the wind direction.

Different aging processes occur between seasons, such as photochemical activity, that could explain the observed amplification of light absorption by rBC around noon. However, the latter effect could not be rigorously demonstrated in this study.

The complexity and diversity of BC mixing states in the real atmosphere cannot be represented in climate models, and therefore these models generally use simplified schemes. A fixed *e*-folding timescale (1–3 d) is commonly used as the turnover time for converting fresh BC particles into aged ones (Myhre et al., 2013). In addition, atmospheric models necessarily approximate the full complexity and diversity of BC composition, which can lead to mismatches with observed E_{abs} (Fierce et al., 2020). The findings presented here suggest that different dynamic processes governing rBC light absorption occur during the day and night and between summer and winter. A parameterization of BC aging explicitly based on aerosol microphysical processes, in which the conversion rate is considered to vary depending on the environmental conditions (e.g., temperature, photochemical activity) and some key species (e.g., aerosol, coating precursors), may be required to accurately represent the true variability in $\mathrm{MAC_{BC}}$.

Data availability. Aerosol microphysical and optical properties are freely available at http://ebas.nilu.no/ (last access: 23 January 2024) (NILU, 2018). CO data are available on the ICOS platform at https://www.icos-cp.eu/ (last access: 23 January 2024). rBC data are available upon request to the authors.

Supplement. The supplement related to this article is available online at: https://doi.org/10.5194/acp-24-1801-2024-supplement.

Author contributions. ST and CD designed the study, developed the analysis protocols and wrote the initial manuscript. PN contributed to the data analysis. FG and VP provided data and methods to analyze them. TB, FG, EL, ST, VP and CD contributed to the measurement campaign. All authors reviewed the final manuscript.

Competing interests. The contact author has declared that none of the authors has any competing interests.

Disclaimer. Publisher's note: Copernicus Publications remains neutral with regard to jurisdictional claims made in the text, published maps, institutional affiliations, or any other geographical representation in this paper. While Copernicus Publications makes every effort to include appropriate place names, the final responsibility lies with the authors.

Acknowledgements. We thank the staff of the Pic du Midi platform (Observatoire Midi-Pyrénées) for their technical assistance. We acknowledge the SNO ICOS-France and ACTRIS-France for supporting greenhouse gas and aerosol observations at PDM and data collection, processing and dissemination. We also acknowledge the use of the HYSPLIT model and READY website from the NOAA Air Resources Laboratory (https://www.ready.noaa.gov/index.php, last access: 23 January 2024). The authors would like to thank the reviewers for their useful comments, which helped to improve the quality of the document. A final acknowledgement goes to Martin Gysel Beer, who brought his expertise to reviewing this paper.

Financial support. This work received funding from the French national program LEFE/INSU and Météo-France. Observation data were collected at the Pyrenean Platform for Observation of the Atmosphere (P2OA; http://p2oa.aero.obs-mip.fr, last access: 23 January 2024). P2OA facilities and staff are funded and supported by the University Toulouse III – Paul Sabatier, France, and CNRS (Centre National de la Recherche Scientifique).

Review statement. This paper was edited by Andreas Petzold and reviewed by three anonymous referees.

References

Adachi, K. and Buseck, P. R.: Changes of ns-soot mixing states and shapes in an urban area during CalNex, J. Geophys. Res.-Atmos., 118, 3723–3730, https://doi.org/10.1002/jgrd.50321, 2013.

Adachi, K., Chung, S. H., Friedrich, H., and Buseck, P. R.: Fractal parameters of individual soot particles determined using electron tomography: Implications for optical properties, J. Geophys. Res.-Atmos., 112, D14202, https://doi.org/10.1029/2006JD008296, 2007.

Adachi, K., Chung, S. H., and Buseck, P. R.: Shapes of soot aerosol particles and implications for their effects on climate, J. Geophys. Res.-Atmos., 115, D15206, https://doi.org/10.1029/2009JD012868, 2010.

Andrews, E., Ogren, J. A., Bonasoni, P., Marinoni, A., Cuevas, E., Rodríguez, S., Sun, J. Y., Jaffe, D. A., Fischer, E. V., Baltensperger, U., Weingartner, E., Coen, M. C., Sharma, S., Macdonald, A. M., Leaitch, W. R., Lin, N. H., Laj, P., Arsov, T., Kalapov, I., Jefferson, A., and Sheridan, P.: Climatology of aerosol radiative properties in the free troposphere, Atmos. Res., 102, 365–393, https://doi.org/10.1016/j.atmosres.2011.08.017, 2011.

Baumgardner, D., Raga, G., Peralta, O., Rosas, I., Castro, T., Kuhlbusch, T., John, A., and Petzold, A.: Diagnosing black carbon trends in large urban areas using carbon monoxide measurements, J. Geophys. Res.-Atmos., 107, ICC 4-1–ICC 4-9, https://doi.org/10.1029/2001JD000626, 2002.

Beeler, P. and Chakrabarty, R. K.: Constraining the particle-scale diversity of black carbon light absorption using a unified framework, Atmos. Chem. Phys., 22, 14825–14836, https://doi.org/10.5194/acp-22-14825-2022, 2022.

Bellouin, N., Quaas, J., Gryspeerdt, E., Kinne, S., Stier, P., Watson-Parris, D., Boucher, O., Carslaw, K. S., Christensen, M., Daniau, A.-L., Dufresne, J.-L., Feingold, G., Fiedler, S., Forster, P., Gettelman, A., Haywood, J. M., Lohmann, U., Malavelle, F., Mauritsen, T., McCoy, D. T., Myhre, G., Mülmenstädt, J., Neubauer, D., Possner, A., Rugenstein, M., Sato, Y., Schulz, M., Schwartz, S. E., Sourdeval, O., Storelvmo, T., Toll, V., Winker, D., and Stevens, B.: Bounding Global Aerosol Radiative Forcing of Climate Change, Rev. Geophys., 58, e2019RG000660, https://doi.org/10.1029/2019RG000660, 2020.

Bergstrom, R. W., Pilewskie, P., Russell, P. B., Redemann, J., Bond, T. C., Quinn, P. K., and Sierau, B.: Spectral absorption properties of atmospheric aerosols, Atmos. Chem. Phys., 7, 5937–5943, https://doi.org/10.5194/acp-7-5937-2007, 2007.

Bey, I., Jacob, D. J., Logan, J. A., and Yantosca, R. M.: Asian chemical outflow to the Pacific in spring: Origins, pathways, and budgets, J. Geophys. Res.-Atmos., 106, 23097–23113, https://doi.org/10.1029/2001JD000806, 2001.

Bond, T. C. and Bergstrom R. W.: Light Absorption by Carbonaceous Particles: An Investigative Review, Aerosol Sci. Tech., 40, 27–67, https://doi.org/10.1080/02786820500421521, 2006.

Bond, T. C., Doherty, S. J., Fahey, D. W., Forster, P. M., Berntsen, T., DeAngelo, B. J., Flanner, M. G., Ghan, S., Kärcher, B., Koch, D., Kinne, S., Kondo, Y., Quinn, P. K., Sarofim, M. C., Schultz, M. G., Schulz, M., Venkataraman, C., Zhang, H., Zhang, S., Bellouin, N., Guttikunda, S. K., Hopke, P. K., Jacobson, M. Z., Kaiser, J. W., Klimont, Z., Lohmann, U., Schwarz, J. P., Shindell, D., Storelvmo, T., Warren, S. G., and Zender, C. S.: Bounding the role of black carbon in the climate system: A scientific assessment, J. Geophys. Res.-Atmos., 118, 5380–5552, https://doi.org/10.1002/jgrd.50171, 2013.

Boucher, O., Balkanski, Y., Hodnebrog, Ø., Myhre, C. L., Myhre, G., Quaas, J., Samset, B. H., Schutgens, N., Stier, P., and Wang, R.: Jury is still out on the radiative forcing by black carbon, P. Natl. Acad. Sci. USA, 113, E5092–E5093, https://doi.org/10.1073/pnas.1607005113, 2016.

Bourgeois, I., Peischl, J., Neuman, J. A., Brown, S. S., Thompson, C. R., Aikin, K. C., Allen, H. M., Angot, H., Apel, E. C., Baublitz, C. B., Brewer, J. F., Campuzano-Jost, P., Commane, R., Crounse, J. D., Daube, B. C., DiGangi, J. P., Diskin, G. S., Emmons, L. K., Fiore, A. M., Gkatzelis, G. I., Hills, A., Hornbrook, R. S., Huey, L. G., Jimenez, J. L., Kim, M., Lacey, F., McKain, K., Murray, L. T., Nault, B. A., Parrish, D. D., Ray, E., Sweeney, C., Tanner, D., Wofsy, S. C., and Ryerson, T. B.: Large contribution of biomass burning emissions to ozone throughout the global remote troposphere, P. Natl. Acad. Sci. USA, 118, e2109628118, https://doi.org/10.1073/pnas.2109628118, 2021.

Bukowiecki, N., Weingartner, E., Gysel, M., Coen, M. C., Zieger, P., Herrmann, E., Steinbacher, M., Gaäggeler, H. W., and Baltensperger, U.: A Review of More than 20 Years of Aerosol Observation at the High Altitude Research Station Jungfraujoch, Switzerland (3580 m a.s.l.), Aerosol Air Qual. Res., 16, 764–788, https://doi.org/10.4209/aaqr.2015.05.0305, 2016.

Cappa, C. D., Onasch, T. B., Massoli, P., Worsnop, D. R., Bates, T. S., Cross, E. S., Davidovits, P., Hakala, J., Hayden, K. L., Jobson, B. T., Kolesar, K. R., Lack, D. A., Lerner, B. M., Li, S.-M., Mellon, D., Nuaaman, I., Olfert, J. S., Petäjä, T., Quinn, P. K., Song, C., Subramanian, R., Williams, E. J., and Zaveri, R. A.: Radiative Absorption Enhancements Due to the Mixing

State of Atmospheric Black Carbon, Science, 337, 1078–1081, https://doi.org/10.1126/science.1223447, 2012.

Cappa, C. D., Kolesar, K. R., Zhang, X., Atkinson, D. B., Pekour, M. S., Zaveri, R. A., Zelenyuk, A., and Zhang, Q.: Understanding the optical properties of ambient sub- and supermicron particulate matter: results from the CARES 2010 field study in northern California, Atmos. Chem. Phys., 16, 6511–6535, https://doi.org/10.5194/acp-16-6511-2016, 2016.

Cappa, C. D., Zhang, X., Russell, L. M., Collier, S., Lee, A. K. Y., Chen, C.-L., Betha, R., Chen, S., Liu, J., Price, D. J., Sanchez, K. J., McMeeking, G. R., Williams, L. R., Onasch, T. B., Worsnop, D. R., Abbatt, J., and Zhang, Q.: Light Absorption by Ambient Black and Brown Carbon and its Dependence on Black Carbon Coating State for Two California, USA, Cities in Winter and Summer, J. Geophys. Res.-Atmos., 124, 1550–1577, https://doi.org/10.1029/2018JD029501, 2019.

Chambers, S. D., Zahorowski, W., Williams, A. G., Crawford, J., and Griffiths, A. D.: Identifying tropospheric baseline air masses at Mauna Loa Observatory between 2004 and 2010 using Radon-222 and back trajectories, J. Geophys. Res.-Atmos., 118, 992–1004, https://doi.org/10.1029/2012JD018212, 2013.

China, S., Mazzoleni, C., Gorkowski, K., Aiken, A. C., and Dubey, M. K.: Morphology and mixing state of individual freshly emitted wildfire carbonaceous particles, Nat. Commun., 4, 2122, https://doi.org/10.1038/ncomms3122, 2013.

China, S., Scarnato, B., Owen, R. C., Zhang, B., Ampadu, M. T., Kumar, S., Dzepina, K., Dziobak, M. P., Fialho, P., Perlinger, J. A., Hueber, J., Helmig, D., Mazzoleni, L. R., and Mazzoleni, C.: Morphology and mixing state of aged soot particles at a remote marine free troposphere site: Implications for optical properties, Geophys. Res. Lett., 42, 1243–1250, https://doi.org/10.1002/2014GL062404, 2015.

Clarke, A. and Kapustin, V.: Hemispheric Aerosol Vertical Profiles: Anthropogenic Impacts on Optical Depth and Cloud Nuclei, Science, 329, 1488–1492, https://doi.org/10.1126/science.1188838, 2010.

Collaud Coen, M., Weingartner, E., Furger, M., Nyeki, S., Prévôt, A. S. H., Steinbacher, M., and Baltensperger, U.: Aerosol climatology and planetary boundary influence at the Jungfraujoch analyzed by synoptic weather types, Atmos. Chem. Phys., 11, 5931–5944, https://doi.org/10.5194/acp-11-5931-2011, 2011.

Collaud Coen, M., Andrews, E., Aliaga, D., Andrade, M., Angelov, H., Bukowiecki, N., Ealo, M., Fialho, P., Flentje, H., Hallar, A. G., Hooda, R., Kalapov, I., Krejci, R., Lin, N.-H., Marinoni, A., Ming, J., Nguyen, N. A., Pandolfi, M., Pont, V., Ries, L., Rodríguez, S., Schauer, G., Sellegri, K., Sharma, S., Sun, J., Tunved, P., Velasquez, P., and Ruffieux, D.: Identification of topographic features influencing aerosol observations at high altitude stations, Atmos. Chem. Phys., 18, 12289–12313, https://doi.org/10.5194/acp-18-12289-2018, 2018.

Croft, B., Lohmann, U., Martin, R. V., Stier, P., Wurzler, S., Feichter, J., Hoose, C., Heikkilä, U., van Donkelaar, A., and Ferrachat, S.: Influences of in-cloud aerosol scavenging parameterizations on aerosol concentrations and wet deposition in ECHAM5-HAM, Atmos. Chem. Phys., 10, 1511–1543, https://doi.org/10.5194/acp-10-1511-2010, 2010.

Denjean, C., Formenti, P., Desboeufs, K., Chevaillier, S., Triquet, S., Maillé, M., Cazaunau, M., Laurent, B., Mayol-Bracero, O. L., Vallejo, P., Quiñones, M., Gutierrez-Molina, I. E., Cassola, F., Prati, P., Andrews, E., and Ogren, J.: Size distribution and optical properties of African mineral dust after intercontinental transport, J. Geophys. Res.-Atmos., 121, 7117–7138, https://doi.org/10.1002/2016JD024783, 2016.

Denjean, C., Brito, J., Libois, Q., Mallet, M., Bourrianne, T., Burnet, F., Dupuy, R., Flamant, C., and Knippertz, P.: Unexpected Biomass Burning Aerosol Absorption Enhancement Explained by Black Carbon Mixing State, Geophys. Res. Lett., 47, e2020GL089055, https://doi.org/10.1029/2020GL089055, 2020.

Drinovec, L., Močnik, G., Zotter, P., Prévôt, A. S. H., Ruckstuhl, C., Coz, E., Rupakheti, M., Sciare, J., Müller, T., Wiedensohler, A., and Hansen, A. D. A.: The "dual-spot" Aethalometer: an improved measurement of aerosol black carbon with real-time loading compensation, Atmos. Meas. Tech., 8, 1965–1979, https://doi.org/10.5194/amt-8-1965-2015, 2015.

Dumont, M., Gascoin, S., Réveillet, M., Voisin, D., Tuzet, F., Arnaud, L., Bonnefoy, M., Bacardit Peñarroya, M., Carmagnola, C., Deguine, A., Diacre, A., Dürr, L., Evrard, O., Fontaine, F., Frankl, A., Fructus, M., Gandois, L., Gouttevin, I., Gherab, A., Hagenmuller, P., Hansson, S., Herbin, H., Josse, B., Jourdain, B., Lefevre, I., Le Roux, G., Libois, Q., Liger, L., Morin, S., Petitprez, D., Robledano, A., Schneebeli, M., Salze, P., Six, D., Thibert, E., Trachsel, J., Vernay, M., Viallon-Galinier, L., and Voiron, C.: Spatial variability of Saharan dust deposition revealed through a citizen science campaign, Earth Syst. Sci. Data, 15, 3075–3094, https://doi.org/10.5194/essd-15-3075-2023, 2023.

Fierce, L., Onasch, T. B., Cappa, C. D., Mazzoleni, C., China, S., Bhandari, J., Davidovits, P., Fischer, D. A., Helgestad, T., Lambe, A. T., Sedlacek, A. J., Smith, G. D., and Wolff, L.: Radiative absorption enhancements by black carbon controlled by particle-to-particle heterogeneity in composition, P. Natl. Acad. Sci. USA, 117, 5196–5203, https://doi.org/10.1073/pnas.1919723117, 2020.

Forrister, H., Liu, J., Scheuer, E., Dibb, J., Ziemba, L., Thornhill, K. L., Anderson, B., Diskin, G., Perring, A. E., Schwarz, J. P., Campuzano-Jost, P., Day, D. A., Palm, B. B., Jimenez, J. L., Nenes, A., and Weber, R. J.: Evolution of brown carbon in wildfire plumes, Geophys. Res. Lett., 42, 4623–4630, https://doi.org/10.1002/2015GL063897, 2015.

Fu, X., Marusczak, N., Heimbürger, L.-E., Sauvage, B., Gheusi, F., Prestbo, E. M., and Sonke, J. E.: Atmospheric mercury speciation dynamics at the high-altitude Pic du Midi Observatory, southern France, Atmos. Chem. Phys., 16, 5623–5639, https://doi.org/10.5194/acp-16-5623-2016, 2016.

Gao, R. S., Schwarz, J. P., Kelly, K. K., Fahey, D. W., Watts, L. A., Thompson, T. L., Spackman, J. R., Slowik, J. G., Cross, E. S., Han, J.-H., Davidovits, P., Onasch, T. B., and Worsnop, D. R.: A Novel Method for Estimating Light-Scattering Properties of Soot Aerosols Using a Modified Single-Particle Soot Photometer, Aerosol Sci. Tech., 41, 125–135, https://doi.org/10.1080/02786820601118398, 2007.

Gao, Y., Chen, F., Lettenmaier, D. P., Xu, J., Xiao, L., and Li, X.: Does elevation-dependent warming hold true above 5000 m elevation? Lessons from the Tibetan Plateau, npj Clim. Atmos. Sci., 1, 1–7, https://doi.org/10.1038/s41612-018-0030-z, 2018.

González-Olabarria, J. R., Mola-Yudego, B., and Coll, L.: Different Factors for Different Causes: Analysis of the Spatial Aggregations of Fire Ignitions in Catalonia (Spain), Risk Anal., 35, 1197–1209, https://doi.org/10.1111/risa.12339, 2015.

Griffiths, A. D., Conen, F., Weingartner, E., Zimmermann, L., Chambers, S. D., Williams, A. G., and Steinbacher, M.: Surface-to-mountaintop transport characterised by radon observations at the Jungfraujoch, Atmos. Chem. Phys., 14, 12763–12779, https://doi.org/10.5194/acp-14-12763-2014, 2014.

Guo, Q., Hu, M., Guo, S., Wu, Z., Peng, J., and Wu, Y.: The variability in the relationship between black carbon and carbon monoxide over the eastern coast of China: BC aging during transport, Atmos. Chem. Phys., 17, 10395–10403, https://doi.org/10.5194/acp-17-10395-2017, 2017.

Gysel, M., McFiggans, G. B., and Coe, H.: Inversion of tandem differential mobility analyser (TDMA) measurements, J. Aerosol Sci., 40, 134–151, https://doi.org/10.1016/j.jaerosci.2008.07.013, 2009.

Healy, R. M., Wang, J. M., Jeong, C.-H., Lee, A. K. Y., Willis, M. D., Jaroudi, E., Zimmerman, N., Hilker, N., Murphy, M., Eckhardt, S., Stohl, A., Abbatt, J. P. D., Wenger, J. C., and Evans, G. J.: Light-absorbing properties of ambient black carbon and brown carbon from fossil fuel and biomass burning sources, J. Geophys. Res.-Atmos., 120, 6619–6633, https://doi.org/10.1002/2015JD023382, 2015.

Henne, S., Brunner, D., Folini, D., Solberg, S., Klausen, J., and Buchmann, B.: Assessment of parameters describing representativeness of air quality in-situ measurement sites, Atmos. Chem. Phys., 10, 3561–3581, https://doi.org/10.5194/acp-10-3561-2010, 2010.

Herrmann, E., Weingartner, E., Henne, S., Vuilleumier, L., Bukowiecki, N., Steinbacher, M., Conen, F., Collaud Coen, M., Hammer, E., Jurányi, Z., Baltensperger, U., and Gysel, M.: Analysis of long-term aerosol size distribution data from Jungfraujoch with emphasis on free tropospheric conditions, cloud influence, and air mass transport, J. Geophys. Res.-Atmos., 120, 9459–9480, https://doi.org/10.1002/2015JD023660, 2015.

Hoyle, C. R., Webster, C. S., Rieder, H. E., Nenes, A., Hammer, E., Herrmann, E., Gysel, M., Bukowiecki, N., Weingartner, E., Steinbacher, M., and Baltensperger, U.: Chemical and physical influences on aerosol activation in liquid clouds: a study based on observations from the Jungfraujoch, Switzerland, Atmos. Chem. Phys., 16, 4043–4061, https://doi.org/10.5194/acp-16-4043-2016, 2016.

Hulin, M., Gheusi, F., Lothon, M., Pont, V., Lohou, F., Ramonet, M., Delmotte, M., Derrien, S., Athier, G., Meyerfeld, Y., Bezombes, Y., Augustin, P., and Ravetta, F.: Observations of Thermally Driven Circulations in the Pyrenees: Comparison of Detection Methods and Impact on Atmospheric Composition Measured at a Mountaintop, J. Appl. Meteorol. Clim., 58, 717–740, https://doi.org/10.1175/JAMC-D-17-0268.1, 2019.

Kanaya, Y., Pan, X., Miyakawa, T., Komazaki, Y., Taketani, F., Uno, I., and Kondo, Y.: Long-term observations of black carbon mass concentrations at Fukue Island, western Japan, during 2009–2015: constraining wet removal rates and emission strengths from East Asia, Atmos. Chem. Phys., 16, 10689–10705, https://doi.org/10.5194/acp-16-10689-2016, 2016.

Kirchstetter, T. W., Novakov, T., and Hobbs, P. V.: Evidence that the spectral dependence of light absorption by aerosols is affected by organic carbon, J. Geophys. Res.-Atmos., 109, D21208, https://doi.org/10.1029/2004JD004999, 2004.

Knox, A., Evans, G. J., Brook, J. R., Yao, X., Jeong, C.-H., Godri, K. J., Sabaliauskas, K., and Slowik, J. G.: Mass Absorption Cross-Section of Ambient Black Carbon Aerosol in Relation to Chemical Age, Aerosol Sci. Tech., 43, 522–532, https://doi.org/10.1080/02786820902777207, 2009.

Ko, J., Krasowsky, T., and Ban-Weiss, G.: Measurements to determine the mixing state of black carbon emitted from the 2017–2018 California wildfires and urban Los Angeles, Atmos. Chem. Phys., 20, 15635–15664, https://doi.org/10.5194/acp-20-15635-2020, 2020.

Kondo, Y., Moteki, N., Oshima, N., Ohata, S., Koike, M., Shibano, Y., Takegawa, N., and Kita, K.: Effects of wet deposition on the abundance and size distribution of black carbon in East Asia, J. Geophys. Res.-Atmos., 121, 4691–4712, https://doi.org/10.1002/2015JD024479, 2016.

Krasowsky, T. S., McMeeking, G. R., Wang, D., Sioutas, C., and Ban-Weiss, G. A.: Measurements of the impact of atmospheric aging on physical and optical properties of ambient black carbon particles in Los Angeles, Atmos. Environ., 142, 496–504, https://doi.org/10.1016/j.atmosenv.2016.08.010, 2016.

Laborde, M., Crippa, M., Tritscher, T., Jurányi, Z., Decarlo, P. F., Temime-Roussel, B., Marchand, N., Eckhardt, S., Stohl, A., Baltensperger, U., Prévôt, A. S. H., Weingartner, E., and Gysel, M.: Black carbon physical properties and mixing state in the European megacity Paris, Atmos. Chem. Phys., 13, 5831–5856, https://doi.org/10.5194/acp-13-5831-2013, 2013.

Laj, P., Bigi, A., Rose, C., Andrews, E., Lund Myhre, C., Collaud Coen, M., Lin, Y., Wiedensohler, A., Schulz, M., Ogren, J. A., Fiebig, M., Gliß, J., Mortier, A., Pandolfi, M., Petäja, T., Kim, S.-W., Aas, W., Putaud, J.-P., Mayol-Bracero, O., Keywood, M., Labrador, L., Aalto, P., Ahlberg, E., Alados Arboledas, L., Alastuey, A., Andrade, M., Artíñano, B., Ausmeel, S., Arsov, T., Asmi, E., Backman, J., Baltensperger, U., Bastian, S., Bath, O., Beukes, J. P., Brem, B. T., Bukowiecki, N., Conil, S., Couret, C., Day, D., Dayantolis, W., Degorska, A., Eleftheriadis, K., Fetfatzis, P., Favez, O., Flentje, H., Gini, M. I., Gregorič, A., Gysel-Beer, M., Hallar, A. G., Hand, J., Hoffer, A., Hueglin, C., Hooda, R. K., Hyvärinen, A., Kalapov, I., Kalivitis, N., Kasper-Giebl, A., Kim, J. E., Kouvarakis, G., Kranjc, I., Krejci, R., Kulmala, M., Labuschagne, C., Lee, H.-J., Lihavainen, H., Lin, N.-H., Löschau, G., Luoma, K., Marinoni, A., Martins Dos Santos, S., Meinhardt, F., Merkel, M., Metzger, J.-M., Mihalopoulos, N., Nguyen, N. A., Ondracek, J., Pérez, N., Perrone, M. R., Petit, J.-E., Picard, D., Pichon, J.-M., Pont, V., Prats, N., Prenni, A., Reisen, F., Romano, S., Sellegri, K., Sharma, S., Schauer, G., Sheridan, P., Sherman, J. P., Schütze, M., Schwerin, A., Sohmer, R., Sorribas, M., Steinbacher, M., Sun, J., Titos, G., Toczko, B., Tuch, T., Tulet, P., Tunved, P., Vakkari, V., Velarde, F., Velasquez, P., Villani, P., Vratolis, S., Wang, S.-H., Weinhold, K., Weller, R., Yela, M., Yus-Diez, J., Zdimal, V., Zieger, P., and Zikova, N.: A global analysis of climate-relevant aerosol properties retrieved from the network of Global Atmosphere Watch (GAW) near-surface observatories, Atmos. Meas. Tech., 13, 4353–4392, https://doi.org/10.5194/amt-13-4353-2020, 2020.

Liu, C., Chung, C. E., Yin, Y., and Schnaiter, M.: The absorption Ångström exponent of black carbon: from numerical aspects, Atmos. Chem. Phys., 18, 6259–6273, https://doi.org/10.5194/acp-18-6259-2018, 2018.

Liu, D., Flynn, M., Gysel, M., Targino, A., Crawford, I., Bower, K., Choularton, T., Jurányi, Z., Steinbacher, M., Hüglin, C., Curtius, J., Kampus, M., Petzold, A., Weingartner, E., Baltensperger,

U., and Coe, H.: Single particle characterization of black carbon aerosols at a tropospheric alpine site in Switzerland, Atmos. Chem. Phys., 10, 7389–7407, https://doi.org/10.5194/acp-10-7389-2010, 2010.

Liu, D., Whitehead, J., Alfarra, M. R., Reyes-Villegas, E., Spracklen, D. V., Reddington, C. L., Kong, S., Williams, P. I., Ting, Y.-C., Haslett, S., Taylor, J. W., Flynn, M. J., Morgan, W. T., McFiggans, G., Coe, H., and Allan, J. D.: Black-carbon absorption enhancement in the atmosphere determined by particle mixing state, Nat. Geosci., 10, 184–188, https://doi.org/10.1038/ngeo2901, 2017.

Liu, D., Ding, S., Zhao, D., Hu, K., Yu, C., Hu, D., Wu, Y., Zhou, C., Tian, P., Liu, Q., Wu, Y., Zhang, J., Kong, S., Huang, M., and Ding, D.: Black Carbon Emission and Wet Scavenging From Surface to the Top of Boundary Layer Over Beijing Region, J. Geophys. Res.-Atmos., 125, e2020JD033096, https://doi.org/10.1029/2020JD033096, 2020.

Liu, F., Yon, J., Fuentes, A., Lobo, P., Smallwood, G. J., and Corbin, J. C.: Review of recent literature on the light absorption properties of black carbon: Refractive index, mass absorption cross section, and absorption function, Aerosol Sci. Tech., 54, 33–51, https://doi.org/10.1080/02786826.2019.1676878, 2020.

Liu, H., Pan, X., Liu, D., Liu, X., Chen, X., Tian, Y., Sun, Y., Fu, P., and Wang, Z.: Mixing characteristics of refractory black carbon aerosols at an urban site in Beijing, Atmos. Chem. Phys., 20, 5771–5785, https://doi.org/10.5194/acp-20-5771-2020, 2020.

Liu, S., Aiken, A. C., Gorkowski, K., Dubey, M. K., Cappa, C. D., Williams, L. R., Herndon, S. C., Massoli, P., Fortner, E. C., Chhabra, P. S., Brooks, W. A., Onasch, T. B., Jayne, J. T., Worsnop, D. R., China, S., Sharma, N., Mazzoleni, C., Xu, L., Ng, N. L., Liu, D., Allan, J. D., Lee, J. D., Fleming, Z. L., Mohr, C., Zotter, P., Szidat, S., and Prévôt, A. S. H.: Enhanced light absorption by mixed source black and brown carbon particles in UK winter, Nat. Commun., 6, 8435, https://doi.org/10.1038/ncomms9435, 2015.

Liu, X., Cheng, Z., Yan, L., and Yin, Z.-Y.: Elevation dependency of recent and future minimum surface air temperature trends in the Tibetan Plateau and its surroundings, Global Planet. Change, 68, 164–174, https://doi.org/10.1016/j.gloplacha.2009.03.017, 2009.

López-Moreno, J. I., El-Kenawy, A., Revuelto, J., Azorín-Molina, C., Morán-Tejeda, E., Lorenzo-Lacruz, J., Zabalza, J., and Vicente-Serrano, S. M.: Observed trends and future projections for winter warm events in the Ebro basin, northeast Iberian Peninsula, Int. J. Climatol., 34, 49–60, https://doi.org/10.1002/joc.3665, 2014.

Mallet, M., Dubovik, O., Nabat, P., Dulac, F., Kahn, R., Sciare, J., Paronis, D., and Léon, J. F.: Absorption properties of Mediterranean aerosols obtained from multi-year ground-based remote sensing observations, Atmos. Chem. Phys., 13, 9195–9210, https://doi.org/10.5194/acp-13-9195-2013, 2013.

Marenco, A., Gouget, H., Nédélec, P., Pagés, J.-P., and Karcher, F.: Evidence of a long-term increase in tropospheric ozone from Pic du Midi data series: Consequences: Positive radiative forcing, J. Geophys. Res.-Atmos., 99, 16617–16632, https://doi.org/10.1029/94JD00021, 1994.

Marusczak, N., Sonke, J. E., Fu, X., and Jiskra, M.: Tropospheric GOM at the Pic du Midi Observatory–Correcting Bias in Denuder Based Observations, Environ. Sci. Technol., 51, 863–869, https://doi.org/10.1021/acs.est.6b04999, 2017.

Matsui, H., Hamilton, D. S., and Mahowald, N. M.: Black carbon radiative effects highly sensitive to emitted particle size when resolving mixing-state diversity, Nat. Commun., 9, 3446, https://doi.org/10.1038/s41467-018-05635-1, 2018.

McMeeking, G. R., Hamburger, T., Liu, D., Flynn, M., Morgan, W. T., Northway, M., Highwood, E. J., Krejci, R., Allan, J. D., Minikin, A., and Coe, H.: Black carbon measurements in the boundary layer over western and northern Europe, Atmos. Chem. Phys., 10, 9393–9414, https://doi.org/10.5194/acp-10-9393-2010, 2010.

McMeeking, G. R., Fortner, E., Onasch, T. B., Taylor, J. W., Flynn, M., Coe, H., and Kreidenweis, S. M.: Impacts of nonrefractory material on light absorption by aerosols emitted from biomass burning, J. Geophys. Res.-Atmos., 119, 12272–12286, https://doi.org/10.1002/2014JD021750, 2014.

Mori, T., Kondo, Y., Ohata, S., Goto-Azuma, K., Fukuda, K., Ogawa-Tsukagawa, Y., Moteki, N., Yoshida, A., Koike, M., Sinha, P. R., Oshima, N., Matsui, H., Tobo, Y., Yabuki, M., and Aas, W.: Seasonal Variation of Wet Deposition of Black Carbon at Ny-Ålesund, Svalbard, J. Geophys. Res.-Atmos., 126, e2020JD034110, https://doi.org/10.1029/2020JD034110, 2021.

Moteki, N.: Climate-relevant properties of black carbon aerosols revealed by in situ measurements: a review, Progress in Earth and Planetary Science, 10, 12, https://doi.org/10.1186/s40645-023-00544-4, 2023.

Moteki, N. and Kondo, Y.: Effects of Mixing State on Black Carbon Measurements by Laser-Induced Incandescence, Aerosol Sci. Technol., 41, 398–417, https://doi.org/10.1080/02786820701199728, 2007.

Moteki, N. and Kondo, Y.: Dependence of Laser-Induced Incandescence on Physical Properties of Black Carbon Aerosols: Measurements and Theoretical Interpretation, Aerosol Sci. Tech., 44, 663–675, https://doi.org/10.1080/02786826.2010.484450, 2010.

Moteki, N., Kondo, Y., Oshima, N., Takegawa, N., Koike, M., Kita, K., Matsui, H., and Kajino, M.: Size dependence of wet removal of black carbon aerosols during transport from the boundary layer to the free troposphere, Geophys. Res. Lett., 39, L13802, https://doi.org/10.1029/2012GL052034, 2012.

Motos, G., Corbin, J. C., Schmale, J., Modini, R. L., Bertò, M., Kupiszewski, P., Baltensperger, U., and Gysel-Beer, M.: Black Carbon Aerosols in the Lower Free Troposphere are Heavily Coated in Summer but Largely Uncoated in Winter at Jungfraujoch in the Swiss Alps, Geophys. Res. Lett., 47, e2020GL088011, https://doi.org/10.1029/2020GL088011, 2020.

Myhre, G. and Samset, B. H.: Standard climate models radiation codes underestimate black carbon radiative forcing, Atmos. Chem. Phys., 15, 2883–2888, https://doi.org/10.5194/acp-15-2883-2015, 2015.

Myhre, G., Samset, B. H., Schulz, M., Balkanski, Y., Bauer, S., Berntsen, T. K., Bian, H., Bellouin, N., Chin, M., Diehl, T., Easter, R. C., Feichter, J., Ghan, S. J., Hauglustaine, D., Iversen, T., Kinne, S., Kirkevåg, A., Lamarque, J.-F., Lin, G., Liu, X., Lund, M. T., Luo, G., Ma, X., van Noije, T., Penner, J. E., Rasch, P. J., Ruiz, A., Seland, Ø., Skeie, R. B., Stier, P., Takemura, T., Tsigaridis, K., Wang, P., Wang, Z., Xu, L., Yu, H., Yu, F., Yoon, J.-H., Zhang, K., Zhang, H., and Zhou, C.: Radiative forcing of the direct aerosol effect from AeroCom Phase II simulations, Atmos. Chem. Phys., 13, 1853–1877, https://doi.org/10.5194/acp-13-1853-2013, 2013.

Müller, T., Laborde, M., Kassell, G., and Wiedensohler, A.: Design and performance of a three-wavelength LED-based total scatter and backscatter integrating nephelometer, Atmos. Meas. Tech., 4, 1291–1303, https://doi.org/10.5194/amt-4-1291-2011, 2011.

Ohata, S., Schwarz, J. P., Moteki, N., Koike, M., Takami, A., and Kondo, Y.: Hygroscopicity of materials internally mixed with black carbon measured in Tokyo, J. Geophys. Res.-Atmos., 121, 362–381, https://doi.org/10.1002/2015JD024153, 2016.

Pan, X. L., Kanaya, Y., Wang, Z. F., Liu, Y., Pochanart, P., Akimoto, H., Sun, Y. L., Dong, H. B., Li, J., Irie, H., and Takigawa, M.: Correlation of black carbon aerosol and carbon monoxide in the high-altitude environment of Mt. Huang in Eastern China, Atmos. Chem. Phys., 11, 9735–9747, https://doi.org/10.5194/acp-11-9735-2011, 2011.

Pandolfi, M., Ripoll, A., Querol, X., and Alastuey, A.: Climatology of aerosol optical properties and black carbon mass absorption cross section at a remote high-altitude site in the western Mediterranean Basin, Atmos. Chem. Phys., 14, 6443–6460, https://doi.org/10.5194/acp-14-6443-2014, 2014.

Pandolfi, M., Alados-Arboledas, L., Alastuey, A., Andrade, M., Angelov, C., Artiñano, B., Backman, J., Baltensperger, U., Bonasoni, P., Bukowiecki, N., Collaud Coen, M., Conil, S., Coz, E., Crenn, V., Dudoitis, V., Ealo, M., Eleftheriadis, K., Favez, O., Fetfatzis, P., Fiebig, M., Flentje, H., Ginot, P., Gysel, M., Henzing, B., Hoffer, A., Holubova Smejkalova, A., Kalapov, I., Kalivitis, N., Kouvarakis, G., Kristensson, A., Kulmala, M., Lihavainen, H., Lunder, C., Luoma, K., Lyamani, H., Marinoni, A., Mihalopoulos, N., Moerman, M., Nicolas, J., O'Dowd, C., Petäjä, T., Petit, J.-E., Pichon, J. M., Prokopciuk, N., Putaud, J.-P., Rodríguez, S., Sciare, J., Sellegri, K., Swietlicki, E., Titos, G., Tuch, T., Tunved, P., Ulevicius, V., Vaishya, A., Vana, M., Virkkula, A., Vratolis, S., Weingartner, E., Wiedensohler, A., and Laj, P.: A European aerosol phenomenology – 6: scattering properties of atmospheric aerosol particles from 28 ACTRIS sites, Atmos. Chem. Phys., 18, 7877–7911, https://doi.org/10.5194/acp-18-7877-2018, 2018.

Park, R. J., Jacob, D. J., Palmer, P. I., Clarke, A. D., Weber, R. J., Zondlo, M. A., Eisele, F. L., Bandy, A. R., Thornton, D. C., Sachse, G. W., and Bond, T. C.: Export efficiency of black carbon aerosol in continental outflow: Global implications, J. Geophys. Res.-Atmos., 110, D11205, https://doi.org/10.1029/2004JD005432, 2005.

Peng, J., Hu, M., Guo, S., Du, Z., Zheng, J., Shang, D., Levy Zamora, M., Zeng, L., Shao, M., Wu, Y.-S., Zheng, J., Wang, Y., Glen, C. R., Collins, D. R., Molina, M. J., and Zhang, R.: Markedly enhanced absorption and direct radiative forcing of black carbon under polluted urban environments, P. Natl. Acad. Sci. USA, 113, 4266–4271, https://doi.org/10.1073/pnas.1602310113, 2016.

Pepin, N., Bradley, R. S., Diaz, H. F., Baraer, M., Caceres, E. B., Forsythe, N., Fowler, H., Greenwood, G., Hashmi, M. Z., Liu, X. D., Miller, J. R., Ning, L., Ohmura, A., Palazzi, E., Rangwala, I., Schöner, W., Severskiy, I., Shahgedanova, M., Wang, M. B., Williamson, S. N., Yang, D. Q., and Mountain Research Initiative EDW Working Group: Elevation-dependent warming in mountain regions of the world, Nat. Clim. Change, 5, 424–430, https://doi.org/10.1038/nclimate2563, 2015.

Pepin, N., Deng, H., Zhang, H., Zhang, F., Kang, S., and Yao, T.: An Examination of Temperature Trends at High Elevations Across the Tibetan Plateau: The Use of MODIS LST to Understand Patterns of Elevation-Dependent Warming, J. Geophys. Res.-Atmos., 124, 5738–5756, https://doi.org/10.1029/2018JD029798, 2019.

Petetin, H., Sauvage, B., Parrington, M., Clark, H., Fontaine, A., Athier, G., Blot, R., Boulanger, D., Cousin, J.-M., Nédélec, P., and Thouret, V.: The role of biomass burning as derived from the tropospheric CO vertical profiles measured by IAGOS aircraft in 2002–2017, Atmos. Chem. Phys., 18, 17277–17306, https://doi.org/10.5194/acp-18-17277-2018, 2018.

Petzold, A., Ogren, J. A., Fiebig, M., Laj, P., Li, S.-M., Baltensperger, U., Holzer-Popp, T., Kinne, S., Pappalardo, G., Sugimoto, N., Wehrli, C., Wiedensohler, A., and Zhang, X.-Y.: Recommendations for reporting "black carbon" measurements, Atmos. Chem. Phys., 13, 8365–8379, https://doi.org/10.5194/acp-13-8365-2013, 2013.

Pierce, J. R., Croft, B., Kodros, J. K., D'Andrea, S. D., and Martin, R. V.: The importance of interstitial particle scavenging by cloud droplets in shaping the remote aerosol size distribution and global aerosol-climate effects, Atmos. Chem. Phys., 15, 6147–6158, https://doi.org/10.5194/acp-15-6147-2015, 2015.

Rangwala, I.: Amplified water vapour feedback at high altitudes during winter, Int. J. Climatol., 33, 897–903, https://doi.org/10.1002/joc.3477, 2013.

Réveillet, M., Dumont, M., Gascoin, S., Lafaysse, M., Nabat, P., Ribes, A., Nheili, R., Tuzet, F., Ménégoz, M., Morin, S., Picard, G., and Ginoux, P.: Black carbon and dust alter the response of mountain snow cover under climate change, Nat. Commun., 13, 5279, https://doi.org/10.1038/s41467-022-32501-y, 2022.

Saleh, R., Adams, P. J., Donahue, N. M., and Robinson, A. L.: The interplay between assumed morphology and the direct radiative effect of light-absorbing organic aerosol, Geophys. Res. Lett., 43, 8735–8743, https://doi.org/10.1002/2016GL069786, 2016.

Samset, B. H. and Myhre, G.: Climate response to externally mixed black carbon as a function of altitude, J. Geophys. Res.-Atmos., 120, 2913–2927, https://doi.org/10.1002/2014JD022849, 2015.

Samset, B. H., Myhre, G., Herber, A., Kondo, Y., Li, S.-M., Moteki, N., Koike, M., Oshima, N., Schwarz, J. P., Balkanski, Y., Bauer, S. E., Bellouin, N., Berntsen, T. K., Bian, H., Chin, M., Diehl, T., Easter, R. C., Ghan, S. J., Iversen, T., Kirkevåg, A., Lamarque, J.-F., Lin, G., Liu, X., Penner, J. E., Schulz, M., Seland, Ø., Skeie, R. B., Stier, P., Takemura, T., Tsigaridis, K., and Zhang, K.: Modelled black carbon radiative forcing and atmospheric lifetime in AeroCom Phase II constrained by aircraft observations, Atmos. Chem. Phys., 14, 12465–12477, https://doi.org/10.5194/acp-14-12465-2014, 2014.

Sanroma, E., Palle, E., and Sanchez-Lorenzo, A.: Long-term changes in insolation and temperatures at different altitudes, Environ. Res. Lett., 5, 024006, https://doi.org/10.1088/1748-9326/5/2/024006, 2010.

Schill, G. P., Froyd, K. D., Bian, H., Kupc, A., Williamson, C., Brock, C. A., Ray, E., Hornbrook, R. S., Hills, A. J., Apel, E. C., Chin, M., Colarco, P. R., and Murphy, D. M.: Widespread biomass burning smoke throughout the remote troposphere, Nat. Geosci., 13, 422–427, https://doi.org/10.1038/s41561-020-0586-1, 2020.

Schuster, G. L., Dubovik, O., and Arola, A.: Remote sensing of soot carbon – Part 1: Distinguishing different absorb-

ing aerosol species, Atmos. Chem. Phys., 16, 1565–1585, https://doi.org/10.5194/acp-16-1565-2016, 2016.

Schwarz, J. P., Gao, R. S., Fahey, D. W., Thomson, D. S., Watts, L. A., Wilson, J. C., Reeves, J. M., Darbeheshti, M., Baumgardner, D. G., Kok, G. L., Chung, S. H., Schulz, M., Hendricks, J., Lauer, A., Kärcher, B., Slowik, J. G., Rosenlof, K. H., Thompson, T. L., Langford, A. O., Loewenstein, M., and Aikin, K. C.: Single-particle measurements of midlatitude black carbon and light-scattering aerosols from the boundary layer to the lower stratosphere, J. Geophys. Res.-Atmos., 111, D16207, https://doi.org/10.1029/2006JD007076, 2006.

Schwarz, J. P., Spackman, J. R., Fahey, D. W., Gao, R. S., Lohmann, U., Stier, P., Watts, L. A., Thomson, D. S., Lack, D. A., Pfister, L., Mahoney, M. J., Baumgardner, D., Wilson, J. C., and Reeves, J. M.: Coatings and their enhancement of black carbon light absorption in the tropical atmosphere, J. Geophys. Res.-Atmos., 113, D03203, https://doi.org/10.1029/2007JD009042, 2008.

Schwarz, J. P., Spackman, J. R., Gao, R. S., Perring, A. E., Cross, E., Onasch, T. B., Ahern, A., Wrobel, W., Davidovits, P., Olfert, J., Dubey, M. K., Mazzoleni, C., and Fahey, D. W.: The Detection Efficiency of the Single Particle Soot Photometer, Aerosol Sci. Tech., 44, 612–628, https://doi.org/10.1080/02786826.2010.481298, 2010.

Schwarz, J. P., Gao, R. S., Perring, A. E., Spackman, J. R., and Fahey, D. W.: Black carbon aerosol size in snow, Sci. Rep.-UK, 3, 1356, https://doi.org/10.1038/srep01356, 2013.

Sedlacek, A. J. I., Lewis, E. R., Onasch, T. B., Zuidema, P., Redemann, J., Jaffe, D., and Kleinman, L. I.: Using the Black Carbon Particle Mixing State to Characterize the Lifecycle of Biomass Burning Aerosols, Environ. Sci. Technol., 56, 14315–14325, https://doi.org/10.1021/acs.est.2c03851, 2022.

Shiraiwa, M., Kondo, Y., Moteki, N., Takegawa, N., Sahu, L. K., Takami, A., Hatakeyama, S., Yonemura, S., and Blake, D. R.: Radiative impact of mixing state of black carbon aerosol in Asian outflow, J. Geophys. Res.-Atmos., 113, D24210, https://doi.org/10.1029/2008JD010546, 2008.

Sorensen, C. M., Yon, J., Liu, F., Maughan, J., Heinson, W. R., and Berg, M. J.: Light scattering and absorption by fractal aggregates including soot, J. Quant. Spectrosc. Ra., 217, 459–473, https://doi.org/10.1016/j.jqsrt.2018.05.016, 2018.

Spackman, J. R., Gao, R. S., Neff, W. D., Schwarz, J. P., Watts, L. A., Fahey, D. W., Holloway, J. S., Ryerson, T. B., Peischl, J., and Brock, C. A.: Aircraft observations of enhancement and depletion of black carbon mass in the springtime Arctic, Atmos. Chem. Phys., 10, 9667–9680, https://doi.org/10.5194/acp-10-9667-2010, 2010.

Srivastava, P., Naja, M., Seshadri, T. R., Joshi, H., Dumka, U. C., Gogoi, M. M., and Babu, S. S.: Implications of Site-specific Mass Absorption Cross-section (MAC) to Black Carbon Observations at a High-altitude Site in the Central Himalaya, Asia-Pac. J. Atmos. Sci., 58, 83–96, https://doi.org/10.1007/s13143-021-00241-6, 2022.

Stein, A. F., Draxler, R. R, Rolph, G. D., Stunder, B. J. B., Cohen, M. D., and Ngan, F.: NOAA's HYSPLIT atmospheric transport and dispersion modeling system, B. Am. Meteor. Soc., 96, 2059–2077, https://doi.org/10.1175/BAMS-D-14-00110.1, 2015.

Sun, H., Biedermann, L., and Bond, T. C.: Color of brown carbon: A model for ultraviolet and visible light absorption by organic carbon aerosol, Geophys. Res. Lett., 34, L17813, https://doi.org/10.1029/2007GL029797, 2007.

Sun, J., Hermann, M., Yuan, Y., Birmili, W., Collaud Coen, M., Weinhold, K., Madueño, L., Poulain, L., Tuch, T., Ries, L., Sohmer, R., Couret, C., Frank, G., Brem, B. T., Gysel-Beer, M., Ma, N., and Wiedensohler, A.: Long-term trends of black carbon and particle number concentration in the lower free troposphere in Central Europe, Environmental Sciences Europe, 33, 47, https://doi.org/10.1186/s12302-021-00488-w, 2021.

Sun, J., Wang, Z., Zhou, W., Xie, C., Wu, C., Chen, C., Han, T., Wang, Q., Li, Z., Li, J., Fu, P., Wang, Z., and Sun, Y.: Measurement report: Long-term changes in black carbon and aerosol optical properties from 2012 to 2020 in Beijing, China, Atmos. Chem. Phys., 22, 561–575, https://doi.org/10.5194/acp-22-561-2022, 2022.

Szopa, S., Naik, V., Adhikary, B., Artaxo, P., Berntsen, T., Collins, W., Fuzzi, S., Gallardo, L., Kiendler-Scharr, A., Klimont, Z., Liao, H., Unger, N., Zanis, P., and Kuo, C.: Short-Lived Climate Forcers, in: AGU Fall Meeting Abstracts, vol. 2021, New Orleans, LA, 13-17 December 2021, Bibcode id. U13B-06, 2021.

Taylor, J. W., Allan, J. D., Allen, G., Coe, H., Williams, P. I., Flynn, M. J., Le Breton, M., Muller, J. B. A., Percival, C. J., Oram, D., Forster, G., Lee, J. D., Rickard, A. R., Parrington, M., and Palmer, P. I.: Size-dependent wet removal of black carbon in Canadian biomass burning plumes, Atmos. Chem. Phys., 14, 13755–13771, https://doi.org/10.5194/acp-14-13755-2014, 2014.

Textor, C., Schulz, M., Guibert, S., Kinne, S., Balkanski, Y., Bauer, S., Berntsen, T., Berglen, T., Boucher, O., Chin, M., Dentener, F., Diehl, T., Easter, R., Feichter, H., Fillmore, D., Ghan, S., Ginoux, P., Gong, S., Grini, A., Hendricks, J., Horowitz, L., Huang, P., Isaksen, I., Iversen, I., Kloster, S., Koch, D., Kirkevåg, A., Kristjansson, J. E., Krol, M., Lauer, A., Lamarque, J. F., Liu, X., Montanaro, V., Myhre, G., Penner, J., Pitari, G., Reddy, S., Seland, Ø., Stier, P., Takemura, T., and Tie, X.: Analysis and quantification of the diversities of aerosol life cycles within AeroCom, Atmos. Chem. Phys., 6, 1777–1813, https://doi.org/10.5194/acp-6-1777-2006, 2006.

Tinorua, S., Denjean, C., Nabat, P., Pont, V., Arnaud, M., Bourrianne, T., Dias Alves, M., and Gardrat, E.: Two-year intercomparison of three methods for measuring black carbon concentration at a high-altitude research station in Europe, EGUsphere [preprint], https://doi.org/10.5194/egusphere-2024-47, 2024.

Tsamalis, C., Ravetta, F., Gheusi, F., Delbarre, H., and Augustin, P.: Mixing of free-tropospheric air with the lowland boundary layer during anabatic transport to a high altitude station, Atmos. Res., 143, 425–437, https://doi.org/10.1016/j.atmosres.2014.03.011, 2014.

Van de Hulst, H.: Light scattering by small particles, John Wiley & Sons, Chapman & Hall, New York, https://doi.org/10.1002/qj.49708436025, 1957.

Wang, Q., Huang, R., Zhao, Z., Cao, J., Ni, H., Tie, X., Zhu, C., Shen, Z., Wang, M., Dai, W., Han, Y., Zhang, N., and Prévôt, A. S. H.: Effects of photochemical oxidation on the mixing state and light absorption of black carbon in the urban atmosphere of China, Environ. Res. Lett., 12, 044012, https://doi.org/10.1088/1748-9326/aa64ea, 2017.

Wei, X., Zhu, Y., Hu, J., Liu, C., Ge, X., Guo, S., Liu, D., Liao, H., and Wang, H.: Recent Progress in Impacts of Mixing State

on Optical Properties of Black Carbon Aerosol, Curr. Pollution Rep., 6, 380–398, https://doi.org/10.1007/s40726-020-00158-0, 2020.

Whiteman, C. D.: Mountain meteorology: fundamentals and applications, Oxford University Press, New York, Oxford, ISBN 978-0-19-756152-2, 2000.

Whittlestone, S. and Zahorowski, W.: Baseline radon detectors for shipboard use: Development and deployment in the First Aerosol Characterization Experiment (ACE 1), J. Geophys. Res.-Atmos., 103, 16743–16751, https://doi.org/10.1029/98JD00687, 1998.

Wittbom, C., Eriksson, A. C., Rissler, J., Carlsson, J. E., Roldin, P., Nordin, E. Z., Nilsson, P. T., Swietlicki, E., Pagels, J. H., and Svenningsson, B.: Cloud droplet activity changes of soot aerosol upon smog chamber ageing, Atmos. Chem. Phys., 14, 9831–9854, https://doi.org/10.5194/acp-14-9831-2014, 2014.

Wong, J. P. S., Tsagkaraki, M., Tsiodra, I., Mihalopoulos, N., Violaki, K., Kanakidou, M., Sciare, J., Nenes, A., and Weber, R. J.: Atmospheric evolution of molecular-weight-separated brown carbon from biomass burning, Atmos. Chem. Phys., 19, 7319–7334, https://doi.org/10.5194/acp-19-7319-2019, 2019.

Xie, C., Xu, W., Wang, J., Liu, D., Ge, X., Zhang, Q., Wang, Q., Du, W., Zhao, J., Zhou, W., Li, J., Fu, P., Wang, Z., Worsnop, D., and Sun, Y.: Light absorption enhancement of black carbon in urban Beijing in summer, Atmos. Environ., 213, 499–504, https://doi.org/10.1016/j.atmosenv.2019.06.041, 2019.

Xu, X., Zhao, W., Qian, X., Wang, S., Fang, B., Zhang, Q., Zhang, W., Venables, D. S., Chen, W., Huang, Y., Deng, X., Wu, B., Lin, X., Zhao, S., and Tong, Y.: The influence of photochemical aging on light absorption of atmospheric black carbon and aerosol single-scattering albedo, Atmos. Chem. Phys., 18, 16829–16844, https://doi.org/10.5194/acp-18-16829-2018, 2018.

Yang, Y., Fu, Y., Lin, Q., Jiang, F., Lian, X., Li, L., Wang, Z., Zhang, G., Bi, X., Wang, X., and Sheng, G.: Re]cent Advances in Quantifying Wet Scavenging Efficiency of Black Carbon Aerosol, Atmosphere, 10, 175, https://doi.org/10.3390/atmos10040175, 2019.

Yttri, K. E., Aas, W., Bjerke, A., Cape, J. N., Cavalli, F., Ceburnis, D., Dye, C., Emblico, L., Facchini, M. C., Forster, C., Hanssen, J. E., Hansson, H. C., Jennings, S. G., Maenhaut, W., Putaud, J. P., and Tørseth, K.: Elemental and organic carbon in PM_{10}: a one year measurement campaign within the European Monitoring and Evaluation Programme EMEP, Atmos. Chem. Phys., 7, 5711–5725, https://doi.org/10.5194/acp-7-5711-2007, 2007.

Yu, P., Froyd, K. D., Portmann, R. W., Toon, O. B., Freitas, S. R., Bardeen, C. G., Brock, C., Fan, T., Gao, R.-S., Katich, J. M., Kupc, A., Liu, S., Maloney, C., Murphy, D. M., Rosenlof, K. H., Schill, G., Schwarz, J. P., and Williamson, C.: Efficient In-Cloud Removal of Aerosols by Deep Convection, Geophys. Res. Lett., 46, 1061–1069, https://doi.org/10.1029/2018GL080544, 2019.

Yuan, J., Modini, R. L., Zanatta, M., Herber, A. B., Müller, T., Wehner, B., Poulain, L., Tuch, T., Baltensperger, U., and Gysel-Beer, M.: Variability in the mass absorption cross section of black carbon (BC) aerosols is driven by BC internal mixing state at a central European background site (Melpitz, Germany) in winter, Atmos. Chem. Phys., 21, 635–655, https://doi.org/10.5194/acp-21-635-2021, 2021.

Yus-Díez, J., Bernardoni, V., Močnik, G., Alastuey, A., Ciniglia, D., Ivančič, M., Querol, X., Perez, N., Reche, C., Rigler, M., Vecchi, R., Valentini, S., and Pandolfi, M.: Determination of the multiple-scattering correction factor and its cross-sensitivity to scattering and wavelength dependence for different AE33 Aethalometer filter tapes: a multi-instrumental approach, Atmos. Meas. Tech., 14, 6335–6355, https://doi.org/10.5194/amt-14-6335-2021, 2021.

Yus-Díez, J., Via, M., Alastuey, A., Karanasiou, A., Minguillón, M. C., Perez, N., Querol, X., Reche, C., Ivančič, M., Rigler, M., and Pandolfi, M.: Absorption enhancement of black carbon particles in a Mediterranean city and countryside: effect of particulate matter chemistry, ageing and trend analysis, Atmos. Chem. Phys., 22, 8439–8456, https://doi.org/10.5194/acp-22-8439-2022, 2022.

Zanatta, M., Gysel, M., Bukowiecki, N., Müller, T., Weingartner, E., Areskoug, H., Fiebig, M., Yttri, K., Mihalopoulos, N., Kouvarakis, G., Beddows, D., Harrison, R., Cavalli, F., Putaud, J., Spindler, G., Wiedensohler, A., Alastuey, A., Pandolfi, M., Sellegri, K., Swietlicki, E., Jaffrezo, J., Baltensperger, U., and Laj, P.: A European aerosol phenomenology-5: Climatology of black carbon optical properties at 9 regional background sites across Europe, Atmos. Environ., 145, 346–364, https://doi.org/10.1016/j.atmosenv.2016.09.035, 2016.

Zanatta, M., Laj, P., Gysel, M., Baltensperger, U., Vratolis, S., Eleftheriadis, K., Kondo, Y., Dubuisson, P., Winiarek, V., Kazadzis, S., Tunved, P., and Jacobi, H.-W.: Effects of mixing state on optical and radiative properties of black carbon in the European Arctic, Atmos. Chem. Phys., 18, 14037–14057, https://doi.org/10.5194/acp-18-14037-2018, 2018.

Zeng, L., Zhang, A., Wang, Y., Wagner, N. L., Katich, J. M., Schwarz, J. P., Schill, G. P., Brock, C., Froyd, K. D., Murphy, D. M., Williamson, C. J., Kupc, A., Scheuer, E., Dibb, J., and Weber, R. J.: Global Measurements of Brown Carbon and Estimated Direct Radiative Effects, Geophys. Res. Lett., 47, e2020GL088747, https://doi.org/10.1029/2020GL088747, 2020.

Zhang, Y., Favez, O., Canonaco, F., Liu, D., Močnik, G., Amodeo, T., Sciare, J., Prévôt, A. S. H., Gros, V., and Albinet, A.: Evidence of major secondary organic aerosol contribution to lensing effect black carbon absorption enhancement, npj Clim. Atmos. Sci., 1, 1–8, https://doi.org/10.1038/s41612-018-0056-2, 2018.

Zhang, Y., Liu, H., Lei, S., Xu, W., Tian, Y., Yao, W., Liu, X., Liao, Q., Li, J., Chen, C., Sun, Y., Fu, P., Xin, J., Cao, J., Pan, X., and Wang, Z.: Mixing state of refractory black carbon in fog and haze at rural sites in winter on the North China Plain, Atmos. Chem. Phys., 21, 17631–17648, https://doi.org/10.5194/acp-21-17631-2021, 2021.

Zhao, Z., Wang, Q., Xu, B., Shen, Z., Huang, R., Zhu, C., Su, X., Zhao, S., Long, X., Liu, S., and Cao, J.: Black carbon aerosol and its radiative impact at a high-altitude remote site on the southeastern Tibet Plateau, J. Geophys. Res.-Atmos., 122, 5515–5530, https://doi.org/10.1002/2016JD026032, 2017.

Zhu, C., Kanaya, Y., Yoshikawa-Inoue, H., Irino, T., Seki, O., and Tohjima, Y.: Sources of atmospheric black carbon and related carbonaceous components at Rishiri Island, Japan: The roles of Siberian wildfires and of crop residue burning in China, Environ. Pollut., 247, 55–63, https://doi.org/10.1016/j.envpol.2019.01.003, 2019.